A hybrid structural health monitoring technique for detection of subtle structural damage

Lakshmi Krishansamy[*] and Rama Mohan Rao Arumulla[a]

*Department of Structural Health Monitoring, CSIR-Structural Engineering Research Centre,
CSIR Road, Taramani, Chennai- 600113, Tamilnadu, India*

Abstract.   There is greater significance in identifying the incipient damages in structures at the time of their initiation as timely rectification of these minor incipient cracks can save huge maintenance cost. However, the change in the global dynamic characteristics of a structure due to these subtle damages are insignificant enough to detect using the majority of the current damage diagnostic techniques. Keeping this in view, we propose a hybrid damage diagnostic technique for detection of minor incipient damages in the structures. In the proposed automated hybrid algorithm, the raw dynamic signatures obtained from the structure are decomposed to uni-modal signals and the dynamic signature are reconstructed by identifying and combining only the uni-modal signals altered by the minor incipient damage. We use these reconstructed signals for damage diagnostics using ARMAX model. Numerical simulation studies are carried out to investigate and evaluate the proposed hybrid damage diagnostic algorithm and their capability in identifying minor/incipient damage with noisy measurements. Finally, experimental studies on a beam are also presented to compliment the numerical simulations in order to demonstrate the practical application of the proposed algorithm.

Keywords: structural health monitoring; empirical mode decomposition; intrinsic mode functions;; cross-correlation; time series analysis; early damage diagnostics; ARMAX; cepstral distance; signal decomposition

1. Introduction

During the past two decades, structural health monitoring has gained importance as a potential research area for civil engineering. Particularly, the focus of the researchers has increased in developing the damage detection techniques using the output-only response with the help of efficient algorithms. Vast amount of literature is available on SHM systems concerned with damage diagnostics of structures (Doebling *et al.* 1998, Das *et al.* 2016), including the range of sensors from optical fiber sensors (Arhant *et al.* 2018) to wireless sensors (Tanner *et al.* 2003). Most of the popularly used vibration-based damage detection methods are modal based and are global in nature, i.e., they use the dynamic properties like natural frequencies and mode shapes (Dorvash 2014). These are obtained for the entire structure from the input-output data using a global structural analysis or through operational modal analysis. Other than these modal based methods, signal based analysis are gaining popularity for damage detection. Techniques based on time-frequency analysis (Pnevmatikos *et al.* 2016, Hsu *et al.* 2014, Rao and Lakshmi 2015), multivariate analysis techniques like PCA (Rao *et al.* 2015) and time series algorithms (Sohn and Farrar 2001, Lakshmi and Rao 2014, Fan *et al.* 2016) are found to be more powerful and promising for damage detection. Even though the above-mentioned techniques have been proved to be successful in detecting damage in various structures and scenarios, it has been shown in later section, of this paper, that they failed to detect the minor/incipient damage (i.e., subtle cracks) in the structure. Nevertheless, the detection of these minor incipient damage remains a challenging task for the following reasons.

i. Feeble changes in few modes: When the incipient damage is small like minor cracks, the minor changes in the dynamic characteristics of the structures developed in the structure, alter only some specific modal responses while other modal responses remain unaltered. Hence the damage features present in the modal response of specific modes due to the minor incipient damage will be insignificantly hidden in the overall response (i.e., the measured dynamic signature).

ii. Environmental and operational variability (EOV) & measurement noise: The presence of the effect of environmental variability which has the capability to alter the dynamic characteristics and signature, mask the existence of the minor incipient damage from diagnosis. The components of the signal that distinguish the various damage classes will be masked by features that characterize the normal operating condition of the structure, particularly when the damage is not yet severe. The effect of measurement noise in the signal conceals the minor damage in the measured signal making it difficult to detect. Even in ideal conditions i.e., there is no variation in normal

---

∗Corresponding author, Ph.D.
  E-mail: lakshmik@serc.res.in
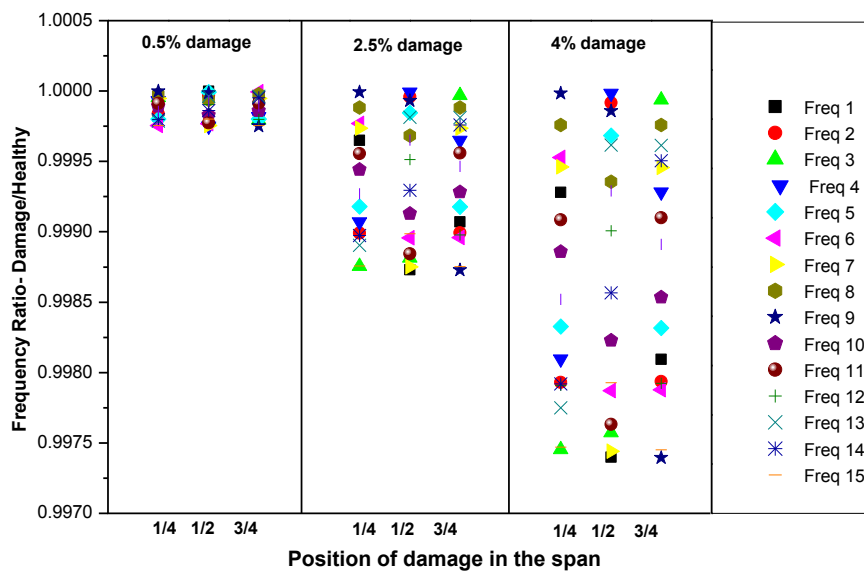[a] Ph.D.
  E-mail: arm2956@yahoo.com

Fig. 1 Variation of modal frequencies with location and severity of damage

operating conditions and also measured signal is noise free, the subtle damages alter only some specific modal responses, keeping others unaltered. In such instances, the global measured signal (i.e., the sum of the responses of all participating modes) likely to mask the minor variations in these limited modal responses. Hence, the general approach for overcoming it involves, in broad terms, proper preprocessing of the raw vibration data records or of the selected characteristic quantity (feature vector), aiming at the removal of the effects of uncertainty.

1.1 Influence of modal frequencies and modal curvatures with severity and spatial location of damage

A minor/incipient damage like a crack in a beam results in reducing mainly the bending stiffness and its effect will be larger on high curvature region. Therefore, the combined effect of position and severity of damage (i.e., crack depth) alter the dynamic characteristics of the structure. For instance, in a simply supported beam, a minor crack near the mid-span, where the curvature of the first mode is maximum and relatively larger crack closer to the support exhibits similar characteristics. In other words, the change in the harmonic content is high at high modal curvature points for minor cracks and can be rather low even for more severe cracks located at low modal curvature points. Hence it is appropriate to detect the modal effective damage rather than the damage itself. This becomes more relevant while dealing with more complex structures.

In order to demonstrate the effect of modal frequencies and mode shapes of the structure to subtle damage, we use a simply supported beam of span 6 m with cross-sectional dimensions as 450 mm X 500 mm. The elastic modulus of the material of the beam is 205 GPa with a mass density of 7950 Kg/m2 and the moment of inertia of 0.000624m4. Since our concern here is to detect minor or subtle damages at their incipient stage, we have considered only minor

damages (varied from 0.5% to 4% damage) in 1/4th span, half span and 3/4th span of the beam. Fig. 1 shows the variation of modal frequencies with severity and location of damage. From Fig. 1, the following observations can be made

i.   The change in the natural frequencies is found insignificant due to minor damage. The maximum change in the frequency for damage levels of 0.5%, 2.0% and 4.0% are found to be of the order 0.0203%, 0.1026%, 0.2081% respectively.

ii. It can also be observed only a set of frequencies are altered (even though insignificantly) while remaining are largely found to be unaltered. This set seems to be consistent with the spatial location of damage irrespective of the severity. Hence we can say from this study the set of these frequencies altered depends rather heavily on the spatial location of damage.

iii. It is also to be pointed out that the above studies have been carried out without considering measurement noise. The measurement noise is expected to completely mask the above observations.

Similarly, the normalized modal curvatures with varying severity of damage and also the spatial location for first 6 modes is shown in Fig. 2. It can be observed from Figs. 1 and 2 that the modal frequencies and their corresponding modes will not exhibit any deviation when the spatial location of damage closer to their respective zero energy node. Hence, it can be concluded that the sensitivity of modal frequencies as well as mode shapes depends on the spatial location of the subtle damage

Keeping this in view in this paper, we attempt to identify modal effective damage rather than damage, by isolating the modes affected by the subtle damage in the structure. In this paper, we attempt a hybrid approach for detecting subtle damages in the structure by preprocessing the data in the first stage to isolate the modal responses
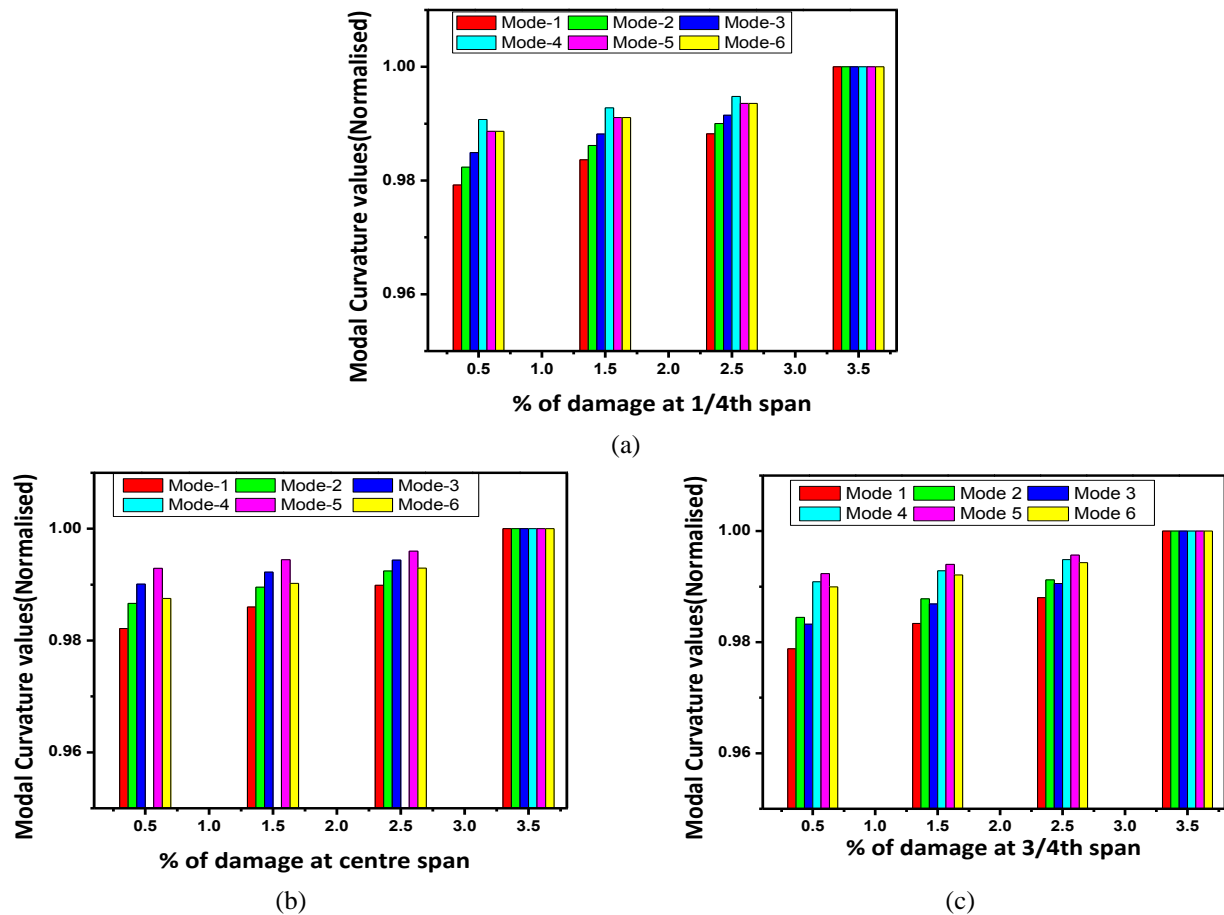
(a)

(b)

(c)

Fig. 2 Normalised modal curvature values for different location and severity of damage

which are been affected by the minor damage using a signal decomposition and reconstruction technique. In this paper, an improved version of Empirical Mode Decomposition (EMD) is employed as a preprocessor to identify and isolate the affected modes from the noisy signals. The reconstructed signal using only the isolated modes (affected by damage) and used in time series analysis. During the process of extracting the minor damage, it becomes mandatory to any technique to handle the effect of environmental variability and measurement noise simultaneously. Since we use time series models in the present work, the uncertainty due to environmental/operational variability can be handled effectively using the look-up table approach by normalization (Farrar *et al.* 2001).

Empirical Mode Decomposition (EMD) (Huang 2014), is popularly being employed to decompose the raw measured time history signals (dynamic signatures) into a finite and often a small number of intrinsic mode functions (IMF). The EMD is highly adaptive and efficient as it is based on the local characteristic time scale of the original data. Therefore, in this paper, we use the empirical mode decomposition technique on the cross-correlated signal to break down the vibration data into a set of uni-modal signals called IMFS. We isolate the IMFs containing significant damage features. These isolated IMFs are used to reconstruct the signal with enriched damage features.

These newly reconstructed signals with enriched damage features are then used for damage diagnostics employing time series models.

The time series models are capable of representing the dynamic properties of the structures like frequency and damping (Pandit and Wu 1983). The coefficients and the prediction errors of the time series models are often famously used to extract the damage features when there is a change in dynamics (Lu and Gao 2005, Mosavi *et al.* 2012, Lakshmi and Rama Mohan Rao 2015). Generally, the statistical characteristics of the responses are affected by the presence of damage. In view of this, the data-driven time series methods using the statistical processing techniques have gained popularity among the vibration based methods (Fassois and Sakellariou 2007, Fassois and Sakellariou 2009, Das e*t al*. 2016). This class of techniques employ the variants of Autoregressive method such as AR (Fugate *et al.* 2001, Jayawardhana *et al.* 2015), ARMA (Nair *et al.* 2006, Hu *et al*. 2015), ARX (Kopsaftopoulos and Fassois 2015, Rosales and Liyanapathirana 2017, Kostić and Gül 2017), AR-ARX (Sohn and Farrar 2001, Zhang 2007), ARMAX (Xie and Mita 2017, Lakshmi and Rao 2016), VARX (Ugalde *et al.* 2015, Sakaris *et al.* 2015), VAR (Mosavi *et al*. 2012, Lakshmi and Rao 2015, Kraemer 2011), ARMAV (Bodeux and Golinval 2001, Foti and Sabia 2010) and time frequency autoregressive moving average (TFARMA) model (Fan *et al.* 2016), Functional pooled models (Sakaris

et al. 2017), LPMAR and TARMA model (Avendaño-Valencia and Fassois 2015). In this paper, ARMAX model is employed as it has a scalar framework with an advantage of the inclusion of the disturbance, unlike the other time series models. The cepstral distance between ARMAX models is used as the damage indicator.

A cepstral distance measure of ARMAX time series models of pristine and the current condition of the structure is used as a damage index to identify the time instant of damage and its spatial location on the structure. With the proposed approach of enhancing the sensitivity of the damage indices by augmenting the EMD to scalar ARMAX model, it is shown robust to locate the subtle damages. Numerical simulation studies have been carried out to test the effectiveness of the proposed algorithm for detecting a small incipient crack in the structure with measurement noise. Experimental studies are also carried out to complement the numerical simulations and also to demonstrate its practical applicability.

2. Cross-correlation of measured time history signals

The presence of measurement noise is inevitable at any measured time history response signal and it cannot be avoided. Hence, an effective damage diagnostic method must have the ability to provide robust damage identification results by extracting suitable features without distorting from the noise present in the measured time history responses.

We can express the measured acceleration time history response (raw dynamic signatures) at any typical spatial location of a structure as follows

$$\tilde{\ddot{Y}}(t) = \ddot{Y}(t) + \zeta(t) \tag{1}$$

in which $\tilde{\ddot{Y}}(t) = [\tilde{\ddot{Y}}_1(t), \ \tilde{\ddot{Y}}_2(t), \tilde{\ddot{Y}}_3(t), \ldots \tilde{\ddot{Y}}_n(t)]^T$ is the measured dynamic signatures (raw acceleration time history signals) of length 'n', $\ddot{Y}(t)$ of the structure. These raw signals are obviously polluted with measurement noise. This noise is generally represented by white Gaussian noise with zero mean and a standard deviation of 1

$$\zeta(t) = [\zeta_1(t), \ \zeta_2(t), \zeta_3(t), \ldots \zeta_n(t)]^T \tag{2}$$

Let us consider two typical spatial locations (sensor nodes) on the structure, say r and s and we can evaluate the cross-correlation function of the measured dynamic signatures (acceleration time history responses) at these two spatial locations.

$$\begin{aligned} R_{rs}\left(\tilde{\ddot{y}}_r(t), \tilde{\ddot{y}}_s(t+\tau)\right) &= E\left[\tilde{\ddot{y}}_r(t), \tilde{\ddot{y}}_s(t+\tau)\right] \\ &= E\left[\left(\ddot{y}_r(t) + \zeta_r(t)\right), \left(\ddot{y}_s(t+\tau) + \zeta_s(t+\tau)\right)\right] \\ &= E\left[\ddot{y}_r(t)\,\ddot{y}_s(t+\tau)\right] + E\left[\ddot{y}_r(t)\,\zeta_s(t+\tau)\right] + \\ &\quad E\left[\ddot{y}_s(t+\tau)\zeta_r(t)\right] + E\left[\zeta_r(t)\zeta_s(t+\tau)\right] \end{aligned} \tag{3}$$

In Eq. (3),

$E\left[\ddot{y}_r(t)\,\zeta_s(t+\tau)\right] = E\left[\ddot{y}_s(t+\tau)\zeta_r(t)\right] = 0$ as the white Gaussian noise is independent of the time history responses, they are uncorrelated.

Similarly, $E\left[\zeta_r(t)\zeta_s(t+\tau)\right] = 0$ when, $\tau \neq 0$ and σ^2, when, $\tau = 0$. σ^2, is the variance of the white Gaussian noise and its value is 1 as the standard deviation of noise is taken as 1. Apart from the measurement noise, the measured dynamic signatures of a structure under ambient excitations are usually more complex and rather difficult to handle. The majority of output-only damage diagnostic techniques are proposed in the literature assumes that either the free vibration response or the impulse response is available for modal identification. Alternatively, in some of the earlier works, it is assumed that the structural vibration response obtained is from white Gaussian noise excitations. However, it is impractical to realize free vibration or impulse response measurements from civil structures as they are usually spatially large with huge mass. Even if it is realizable, we need to suspend the normal operations on the structure, for example, regular traffic needs to be suspended to measure the dynamic signatures. Hence special efforts are needed for the investigation of damage diagnostic methods based on ambient vibration signals.

In reality, both the components of stationary random excitations and nonstationary random excitations will be present in the measured dynamic signatures of the civil structures with the ambient excitations. As mentioned earlier, the ambient excitations on a structure can be assumed to be the sum of stationary random excitations and nonstationary random excitations.

$$f(t) = f_{st}(t) + f_{nst}(t) \tag{4}$$

where $f_{st}(t)$ and $f_{nst}(t)$ are the stationary and non-stationary random excitations respectively.

The nonstationary random excitation $f_{nst}(t)$ can be decomposed further into periodic ($f_{nst}^p(t)$) and aperiodic ($f_{nst}^{\tilde{p}}(t)$) excitations. With this, Eq. (4) can be written as

$$f(t) = f_{st}(t) + f_{nst}^p(t) + f_{nst}^{\tilde{p}}(t) \tag{5}$$

If the value of $E[f_{st}^2(t)]$ is much greater than, $E[f_{nst}^2(t)]$ then we can assume that the structure is subjected to stationary random excitation, otherwise, we need to consider that the predominant forces acting on the structure are nonstationary. In such situations, we may have to resort to appropriate damage diagnostic techniques to handle non-stationary structural response signals.

We can write the structural response at any typical r[th] and the sth nodes of a structure (with n_s sensor nodes), subjected to excitation force f(t), as follows

$$\ddot{y}_r(t) = \ddot{y}_r^{st}(t) + \ddot{y}_r^{p}(t) + \ddot{y}_r^{\tilde{p}}(t);$$
$$\ddot{y}_s(t) = \ddot{y}_s^{st}(t) + \ddot{y}_s^{p}(t) + \ddot{y}_s^{\tilde{p}}(t); \tag{6}$$

where the superscripts 'st', 'p', and $\bar{p}$ refers to the structural response subjected to stationary random excitations, periodic and aperiodic force excitations, respectively.

We can write the cross-correlated response of the two signals given in Eq. (6) as

$$R_{rs}(t_1, t_2) = E\left[\ddot{y}_r(t_1)\ddot{y}_s(t_2)\right]$$
$$= R_{rs}^{st}(t_1, t_2) + R_{rs}^{p}(t_1, t_2) + \bar{r}_{rs}(t_1, t_2) \tag{7}$$

in which

$$R_{rs}^{st}(t_1, t_2) = E\left[\ddot{y}_r^{st}(t_1)\ \ddot{y}_s^{st}(t_2)\right] \tag{8}$$

$$R_{rs}^{p}(t_1, t_2) = E\left[\ddot{y}_r^{p}(t_1)\ \ddot{y}_s^{p}(t_2)\right] \tag{9}$$

$$\bar{r}_{rs}(t_1, t_2) = E\left[\ddot{y}_r(t_1)\ \ddot{y}_s(t_2)\right]$$
$$- E\left[\ddot{y}_r^{st}(t_1)\ \ddot{y}_s^{st}(t_2)\right]$$
$$- E\left[\ddot{y}_r^{p}(t_1)\ \ddot{y}_s^{p}(t_2)\right] \tag{10}$$

The cross-correlation under stationary random excitation component given in Eq. (8) can be written as

$$R_{rs}^{st}(\tau) = E\left[\ddot{y}_r^{st}(t)\ \ddot{y}_s^{st}(t+\tau)\right]$$
$$= \sum_{j=1}^{n_s} B_{rs}^{j} e^{-\zeta^{j}\omega^{j}(t)\tau} sin\left(\omega_d^{j}(t)\tau + \varphi_j\right) \tag{11}$$

where n_s is the number of frequencies excited by the stationary random excitation, B_{rs}^{j} is a coefficient of mode j, associated with nodes r and s. ω^{j} is the jth natural frequency excited due to the stationary random excitations. Similarly, ζ_j, ω_d^{j} and φ_j are the damping ratio, damped natural frequency and the phase angle of the jth mode respectively.

Since the response of a linear structure, subjected to periodic excitation, $f_{nst}^{p}(t)$, will be periodic, with the frequencies same as the excitation frequencies, the cross-correlation of the structural responses at the node, r and node, s , is also periodic and is given as

$$R_{rs}^{p}(\tau) = \sum_{h=n_s+1}^{n_s+k} B_{rs}^{h} e^{-\zeta^{h}\omega^{h}(t)\tau} sin\left(\omega_d^{h}(t)\tau + \varphi_h\right) \tag{12}$$

where k is the number of frequencies excited by the periodic random excitation, ω^{h} is the hth frequency excited due to the periodic excitations. B_{rs}^{h} and φ_h are respectively the amplitude and phase angle associated with h^{th} mode.

It can be observed that Eqs. (11) and (12) have similar expressions which can be represented in a unified manner for $\left(n_s + k\right)$ number of frequencies as

$$R(\tau) = \sum_{j=1}^{n_s+k} C_{rs}^{j} e^{-\zeta^{j}\omega^{j}(t)\tau} sin\left(\omega_d^{j}(t)\tau + \varphi_j\right) \tag{13}$$

where C_{rs}^{j} refers to the amplitude of the jth mode corresponding to the cross-correlated response of nodes r and s. Using Eq. (13) in Eq. (7), we get

$$R_{rs}(\tau) = \sum_{j=1}^{n_s+k} C_{rs}^{j} e^{-\zeta^{j}\ \omega^{j}(t)\tau} sin\left(\omega_d^{j}(t)\tau + \varphi_j\right)$$
$$+ \bar{r}_{rs}(t_1, t_2) \tag{14}$$

We can decompose the cross-correlated acceleration response given in Eq. (14) into a series of IMFs, *M* and a residue, *r,* using empirical mode decomposition as follows.

$$R_{rs}(\tau) = \sum_{j=1}^{n_s+k} M_{rs}^{j}(\tau) + r(\tau); \quad where$$
$$\sum_{j=1}^{n_s+k} M_{rs}^{j}(\tau) = \sum_{j=1}^{n_s+k} C_{rs}^{j} e^{-\zeta^{j}\omega^{j}(t)\tau} sin\left(\omega_d^{j}(t)\tau + \varphi_j\right) \tag{15}$$
$$and \quad r(\tau) = \bar{r}_{rs}(t_1, t_2)$$

The residual part, $r(\tau)$, consists of measurement noise and also the components of the response which do not contain the modal information i.e., response under aperiodic excitations. From this formulation, It is clear that using the cross-correlated responses, the time history response of a structure under ambient excitation (consists of both stationary and nonstationary random excitations) can be decomposed into a series of IMFs using empirical mode decomposition. We also notice that non-modal components of the response including noise can be conveniently isolated to a larger extent using this formulation.

2.1 Empirical mode decomposition

Empirical mode decomposition (Huang 2014) as its name suggests is an empirical method. The aim of this method is to decompose the complicated (non-linear and/or non-stationary) time history response signal into a series of oscillating components obeying some basic properties, called intrinsic mode functions (IMFs). The basic principle in EMD is to decompose a signal *y*(*t*) into a set of zero mean mono-components called the IMFs. In each IMF generated, the number of extreme and the number of zero-crossings can differ at most by one. Further, at each point in

the generated IMF, the mean value defined by local maxima and the local minima must be zero. Sifting is the name given to the empirical procedure associated with EMD. It works as follows: we first identify the local maxima and minima of the measured time history response $y(t)$ and generate upper and lower envelopes by connecting these points through cubic spline interpolation. We later compute the mean of the upper and lower envelopes and subtract from the time history $y(t)$. The difference between the original time history and the mean value, c1, is called the first IMF if it satisfies the two basic criteria discussed above. We repeat the same sifting process on the new time history obtained after subtracting the C1 component from the original signal $y(t)$, in order to generate the second IMF. This process is repeated to generate rest of the IMFs till the residue becomes a monotonic function or less than specified convergence level. We can reconstruct the original time history $y(t)$ by adding up all the IMFs, n_{IMF} including the residue, r_{IMF} as shown in Eq. (16).

$$y(t) = \sum_{j=1}^{n_{IMF}} C_j(t) + r_{IMF}(t) \qquad (16)$$

2.2 Empirical mode decomposition with intermittency

The IMFs generated through the empirical mode decomposition should be complete, adaptive and almost orthogonal decomposition of the original time history signal. However, the sifting process discussed above, cannot produce quality IMFs mainly due to large swings near the ends of the signal. The propagation of these swings inside corrupt the complete signal and it subsequently results in the form of poor IMFS. The large swings near the ends of the signal are basically due to the spline fitting process associated with the sifting.

This will be predominant especially when low-frequency components are present in the signal. Apart from this, in the signals with closely spaced frequency components, the modal perturbation phenomena is too prominent to be ignored and it results in the poor sifting. The IMFs thus generated will generally cover more than one modal frequency and can also have some pseudo components. In order to overcome these limitations, several EMD techniques are proposed in the literature and EMD with intermittency criteria is popular among them

Initially, EMD with intermittency criteria was proposed by (Huang 2005) to locate the intermittent components of the signal. Alternatively, an approach was proposed by (Gao *et al*. 2008) using the Teager-Kaiser energy operator to locate the intermittent components of the signal. Subsequently, several other researchers have investigated on improving the EMD for generating IMFs. Since our objective is to generate the IMFs and to ensure that each of the IMF generated, represent the individual modal response, we have implemented the EMD with intermittency criteria as given below.

Our objective in the present work is to decompose the response signal into IMFs such that each IMF represents one single modal response. In order to accomplish this, we impose an intermittent frequency in the sifting process in order to ensure that each of the IMFs generated to represent the modal response contains only one frequency component. We use a bandpass filter during the sifting process to remove all the frequency components which are lower or greater than from an IMF. We can obtain the frequency components related to each resonant frequency of the structure using FFT. The frequencies corresponding to the modal components of the structure present in the Fourier spectrum are partitioned into several (say m) subdomains. The centre of each subdomain represent the resonant frequency f_k^0. The upper and lower limits of each subdomain (i.e., f_k^u and f_k^l (k = 1, 2, 3,. . . , m) is defined as $(1 \pm 5\%) f_k^0$. Accordingly, the resonant frequency band covered in Fourier spectrum will be divided into nm sub-domains as follows

$$\Omega_j = \left\{ |f| f_i \leq f \leq f_{j+1} \right\} j = 1,2, ...m \qquad (17)$$

We use band-pass filter by considering the boundaries of each subdomain as the sweep starting and sweep-ending frequency limits, to generate a number of narrowband signals from the original signal.

The generated IMFs will have a very good correlation with the original signal as these IMFs contain the frequency components of the original signal. Keeping this in view, we use the correlation strength as a measure to isolate the true IMFs from the other pseudo components. Accordingly, we compute the correlation coefficient, $\mu_i, (i = 1, 2, ..., n_{IMF})$ of each of the IMFs with the signal as follows.

Correlation Coefficient,

$$\mu_i = \frac{1}{N-1} \sum_{j=1}^{N} \left(\frac{A_j - \Omega_A}{\overline{\sigma}_A} \right) \left(\frac{B_j - \Omega_B}{\overline{\sigma}_B} \right) \qquad (18)$$

where A is the IMF, B is the original signal, N is the sample size, Ω and $\overline{\sigma}$ are used to indicate the mean and standard deviation respectively.

We normalize the signal and also the IMFs before computing the correlation coefficients, by dividing them with their respective maximum values. This normalization helps in retaining some of the low amplitude real IMFs. In order to differentiate the true IMFs from pseudo IMFs, we use the correlation coefficients with a threshold ϑ defined as, $\vartheta = \max(\mu_i) / \kappa$ (i=1........n_{IMF}), where κ is an assumed empirical factor and should be greater than 1.0.

We retain the IMFs, if $\mu_i \geq \vartheta$, otherwise, we eliminate by adding to the residue. The main objective here is to guarantee that the selected IMFs include all the resonant modes to be extracted and have no pseudo-components. In the present work, κ is assumed as 10.0.

Apart from this, we use the signal extension method employing time series to eliminate the end effects of IMFs

generated. As mentioned earlier, the end effects of sifting disturb the EMD process quite significantly. In order to handle these end effects, several distinct approaches are suggested in the literature. We can classify them broadly as signal extension approaches with or without damping and extrema extension techniques (Shen *et al.* 2005). However, most of these techniques suggested to handle the end effects associated with periodic or quasi-periodic signals. They are not found to be effective for non-stationary and transient signals. Keeping this in view, in this paper, we use a signal extension technique based on the autoregressive model. The details of the signal extension technique are as follows:

Let $Y = [y(t_1), y(t_2), ..., y(t_n)]$ be a time series of size n, and $Y_{ext} = [y(t_{n+1}), ..., y(t_{n+n_e})]$, the extrapolated signal of size n_e can be computed as follows:

Shift the mean of the signal, Y, to zero, according to the average calculated with the last p points as $Y_s = Y - \mu$, where $\mu = mean[y(t_{n-p}), y(t_{n-p+1}), ..., y(t_n)]$ is an average of the last p points. Then the extrapolated points Y_{ext} are calculated recursively using the two preceding points as

$$y_s(t_i) = \beta_1 \cdot y_s(t_{i-1}) + \beta_2 \cdot y_s(t_{i-2})$$
$$\forall i \in \{(n+1), ..., n+n_e\}, \tag{19}$$

$$Y_{ext} = (y(t_{n+1}), y(t_{n+2}) ...., y(t_{n+n_e}))$$
$$= (y_s(t_{n+1}), y_s(t_{n+2}) ...., y_s(t_{n+n_e})) + \overline{y} \tag{20}$$

where the coefficients β_1 and β_2 can be computed as

$$\beta_1 = \frac{2 - (\omega_s \Delta t)^2}{1 + \zeta \frac{\Delta t}{2}}; \beta_2 = \frac{1 - \zeta \frac{\Delta t}{2}}{1 + \zeta \frac{\Delta t}{2}}; \tag{21}$$

ω_s is the pulsation of the sinusoidal extension and it is determined using the time scale defined by the nearest local extrema as

$$\omega_s = \begin{cases} \dfrac{\pi}{|T|} & \text{if } T \geq 4\Delta t \\ \dfrac{\pi}{4\Delta t} & \text{otherwise} \end{cases} \tag{22}$$

where T is the difference between the two-time instants of last two extrema in the time series, Δt is the time step length i.e., $t_2 - t_1$. ζ is the damping coefficient taken as 0.001. It should be mentioned here that ω_s is calculated based on the suggestion of (Coughlin and Tung 2005). However, T should be greater than four times the time step to prevent the auto-regressive time series model

from diverging to infinity. Hence, if T is less than $4\Delta t$, T is taken as $4\Delta t$ in the Eq. (22). It is appropriate to mention here that the phase and the amplitude of the sinusoidal extension are automatically adjusted by the auto-regressive model. This technique is found to be appropriate to flatten the envelopes without creating any artificial periodicity in the low-frequency IMFs.

Under the minor/early damage circumstances, among all the true IMFs, only a few IMFs contain the information of damage as only a few modes are affected by the damage. In order to isolate the IMFs related to the modes, which are really affected by the damage, an automated algorithm is used in this work and is described below.

2.3 Automated algorithm to choose the IMFs for damage diagnosis

The IMFs extracted by EMD process are the mono-component responses of the original signal. The sum of all the IMFs and the residue gives the original measured time-history response. Therefore, every true IMF is expected to have a good correlation with the measured time-history response as it is a part of the total response. When a current signal from the damaged state of the structure is measured and subjected to EMD, the extracted IMFs, which are mono-component signals, are expected to correlate well with the measured current signal, but not with any other healthy baseline signals. This feature is exploited to choose the relevant IMFs which can reflect on the altered dynamic properties due to damage.

The following steps are adopted to isolate the IMFs containing the damage information among the true IMFs.

i. The dynamic signatures i.e., acceleration time history responses, obtained from the current state of the structure, y(t) (i.e., with damage) are decomposed into M IMFs using EMD. The IMFs obtained are denoted as $C_i(t)$, $(i = 1, 2, ..., n_{IMF})$

ii. Similarly, the reference dynamic signatures x(t), i.e., responses from a healthy state of the structure, chosen using the matching technique discussed earlier are also decomposed into IMFs and are denoted as $R_i(t)$, $(i = 1, 2, ..., n_{IMF})$.

iii. Compute the correlation coefficients γ_i^j, $(i = 1, 2, ..., n_{IMF}; j = 1, 2, ...n_s)$ of the current IMFs, $C_i(t)$ and measured time history responses x(t) of the reference condition.

iv. Similarly compute the correlation coefficients η_i^j, of the current IMFs, $C_i(t)$ and measured time history responses y(t) of the current state.

v. Compute the difference in the corresponding correlation coefficients for all sensors, n_s

$$\xi_i^j = \eta_i^j - \gamma_i^j; \binom{i = 1, 2, ...n_{IMF}}{j = 1, 2, ...n_s} \tag{23}$$

vi. Compute damage feature(DF) index of each current IMF

$$DF(i) = MAX(\xi_i^j); \begin{pmatrix} i = 1, 2, \dots n_{IMF} \\ j = 1, 2, \dots n_s \end{pmatrix} \quad (24)$$

vii. Sort the DF vector and choose the sorted top few modal time history responses with higher values of damage feature index, based on user-defined cut-off. A cut-off value of 0.8 is defined for all the numerical studies.

viii. Similarly, reconstruct the reference and current time history responses, $\tilde{x}_i(t)$ and $\tilde{y}_i(t)$ ($i = 1, 2, 3.. \ n_s$) by choosing the modal time history responses of the modes chosen in step (vii)

ix. Use these reconstructed current time history data, $\tilde{y}(t)$ and reference time history data, $\tilde{x}(t)$ for computing the spatial damage in the structure using the ARMAX model.

The details of ARMAX model and the cepstral distance measure are given in Appendix-A for readers' benefit and hence not explained in this section.

3. Damage detection methodology

A damage detection technique combining EMD and time series analysis is proposed to detect the damage in the structural system at its earliest stage of incipience. The proposed technique is an output-only damage detection method and utilizes the acceleration time-history data from the sensors placed on the structure of interest. The process of damage detection is carried out in two phases namely: preliminary phase and testing phase.

The proposed damage diagnostic algorithm is carried out by following the step by step procedure as given below:

Preliminary Phase:

1. The measured vibration data, X (i.e., acceleration time-history responses) recorded for time, *'t'*, from all the sensors placed on an undamaged (healthy) structure, is segmented into blocks of data of finite duration, whose elements are denoted by $x_{ij}(t); \ i = 1, \dots, n_s; \ j = 1, \dots, M$, where n_s is the number of sensors and M is the number of data blocks. Populate a database with these baseline signals.

2. Fit an ARMAX model shown in Eq. (A.1) to the subsets of the baseline data for all i and j

Testing Phase:

3. Obtain new acceleration signal (current data), Y for time 't', from a potentially damaged structure for all the sensors and segment it into finite blocks of data, whose elements are denoted by

$y_{ij}(t); \ i = 1, \dots, n_s; \ j = 1, \dots, M$ (similar to step 1).

4. Fit an ARMAX model to the current data (similar to step 2)

$$y(t) = \sum_{i=1}^{p} \alpha_i \, y(t-i)$$
$$+ \sum_{i=1}^{q} \beta_i u(t - n_k - i) \quad (25)$$
$$+ \sum_{i=1}^{b} \delta_i \varepsilon(t-i) + \varepsilon(t)$$

5. Perform normalization by matching:
   For each sensor i, every data-block of the current data is matched with a data-block of the signal in the baseline pool using the minimization of the value "*Difference*" as given below.

$$Difference = \sum_{k=1}^{p} \left(\alpha_k^x - \alpha_k^y \right)^2 \quad (26)$$

Choose the data segment, q of the baseline data, $x(t)$ whose AR coefficients match closely with the AR coefficients of the current data (i.e., the '*Difference*' in Eq. (26) is minimum) and use it for all the subsequent computations

6. Perform empirical mode decomposition on the matched subsets of baseline and current data and obtain the IMFs independently. Choose the IMFs with rich damage sensitive features through the automated algorithm defined in section 2.3.

7. Add up all the selected modal responses to obtain reconstructed time history responses, $\tilde{y}_i(t)$ ($i = 1, 2, 3.. \ n_s$) corresponding to current data, with damage rich features. The number of modal responses considered for reconstruction can be from one to maximum of m modes. Similarly, reconstruct the reference time history responses, using the modal time history responses chosen in step 6.

8. Fit ARMAX model to the new reference and current data subsets and evaluate the damage index using the cepstral distances of the two models, described in section 2.5.

9. Plot the cepstral distance damage index for every sensor, to visualize the spatial location of damage. The sensor nodes which indicate the highest magnitudes of the damage index reveal the location of damage precisely. For the benefit of the reader, a flowchart of the proposed methodology is presented in Fig. 3.
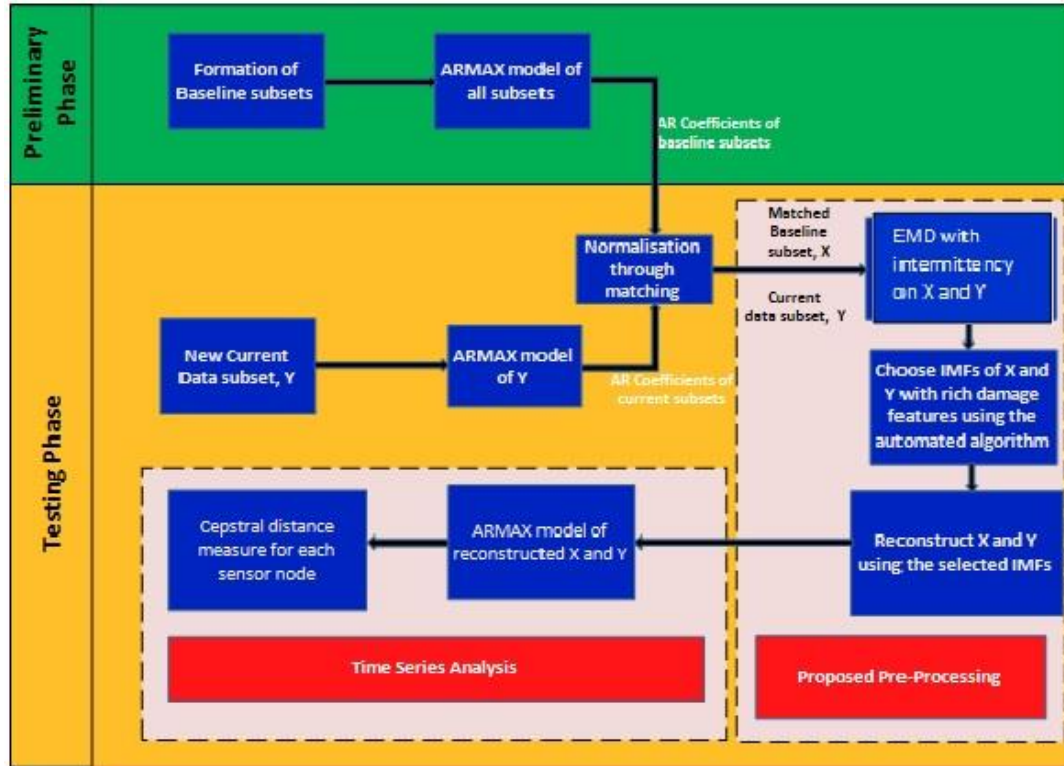
Fig. 3 Flowchart of the proposed technique

4. Validation studies

The effectiveness of the proposed EMD augmented ARMAX model is demonstrated with an example of a simply supported elastic beam. Transverse elasto-plastic cracks are generated on the beam on loading and a cracked beam finite element analysis is used to obtain the time history responses. The initiation of cracks are perceived as the incipience of damage and the proposed EMD-ARMAX technique is applied to identify the spatial location. Apart from the numerical simulation studies, an experimental verification is also carried out using an RCC beam inflicted with cracks due to static loads.

4.1 Numerical verification using a simply supported beam

The simulated numerical example used for validation studies is a simply supported beam girder, with dimensions of 10000 mmx450 mmx550 mm, which is in a healthy state initially. The simply supported beam with the material properties is shown in Fig. 4(a). The beam is discretized into 20 elements for the simulation studies. The beam is assumed to carry accelerometers on 19 nodes, eliminating the nodes at the supports.

4.1.1 Generation of baseline data:
A stochastic random dynamic loading is simulated for exciting the beam. Newmark's time marching scheme is used in finite element analysis to compute the acceleration time history response with a sampling rate of 2000 Hz.

Initially, 12s long acceleration time history data are generated with random loads and normal operational conditions. A time-history of a typical random load and its frequency spectrum are shown in Figs. 4(b) and 4(c) respectively.

Most of the structural damage diagnostic techniques show great sensitivity to noise when they are applied to real situations. Therefore, the performance of the proposed technique has to be verified with respect to the immunity towards measurement noise. In order to investigate the effect of measurement noise, we have contaminated the computed time history measurements with zero mean white Gaussian noise. The noisy measurements have been obtained by adding a normal random component to the computed noise free acceleration time history response as

$$\tilde{x}_m = \tilde{x} + \delta_p N_{noise}\sigma(\tilde{x}) \qquad (27)$$

where δ_p is the percentage noise level, N_{noise} is the standard normal distribution vector with zero mean and unit standard distribution, $\sigma(\tilde{x})$ is the standard deviation of the noise-free measured (computed) time history response. The random noise levels of 5%, are considered in the present investigations. Severe experimental conditions are simulated by maintaining the correlations of noisy sequences of different nodes as low as possible. This healthy data generated with 5% measurement noise is segmented into 50 subsets with 1000 samples in each.
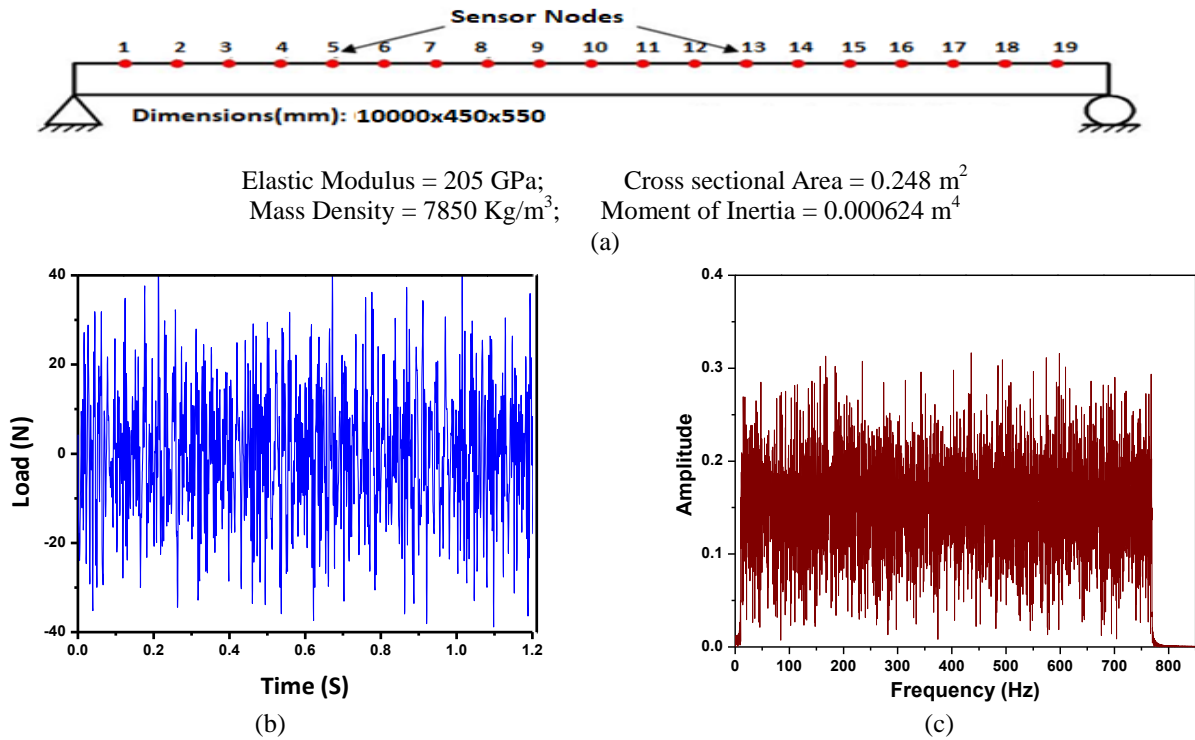
Elastic Modulus = 205 GPa;   Cross sectional Area = 0.248 m^2
Mass Density = 7850 Kg/m^3;   Moment of Inertia = 0.000624 m^4

(a)

(b)

(c)

Fig. 4 (a) A Simply supported beam, (b) typical load time-history and (c) Fourier spectrum of load time-history

4.1.2 Generation of test data:

Similarly, the acceleration data for the current state of the structure, with the simulated damage as shown in Table 1, by introducing cracks of a specified length, on selected elements are generated and segmented into subsets. The formulations of the finite element analysis of the cracked beam, proposed by (Krawczuk *et al.* 2000), are used in the present work to obtain the vibration responses after damage. The formulations of stiffness and mass matrices are given in Appendix –B for the benefit of the readers.

By using Eqs. (B.1)-(B.3), the acceleration responses are generated to form the current data in a way that initially, the structure is healthy and the damage is initiated after few instants of time. To simulate this scenario, the damage is introduced after 3 seconds (i.e., in the 7th current subset data).

Table 1 Test cases for damage detection of simply supported beam

Test case	Depth of crack	Location of crack	Time instant of damage
1. Single crack	10 mm	2/3rd length of the 6th element	6000th time step
2. Multiple cracks	10 mm	(i) 2/3rd length of the 6th element	10000th time step
	15 mm	(ii) Middle of the 15th element	

4.1.3 Detection using existing popular techniques

Initially, the ability of the existing popular vibration-based damage detection techniques to detect subtle cracks in the structure is investigated in this section, using the subsets of the test case-1 shown in Table 1. For this purpose, selected popularly used damage detection techniques are considered. The techniques employed in the present investigation here are: Principal Component Analysis (PCA) (Golinval 2017), Hilbert Huang Transform (HHT) (Rao and Lakshmi 2015), Wavelet transformation (Pnevmatikos 2010) and finally time series models using AR-ARX model (Lakshmi and Rao 2015) and ARMAX model (Lakshmi and Rao 2016). We have presented the curvature of the PCA modes in Fig. 5. It is clear from the first three PCA modes (chosen based on energy criteria) shown in Fig. 5, that there is no abnormality in the form of a sudden spike at the spatial location of damage and also there is no visible variation between the healthy structure and the one with minor crack (test case-1 shown in Table1). We further demonstrate here that the Hilbert Huang transform also fails to detect the minor incipient cracks in the structure. Fig. 6 shows the instantaneous envelope of the beam for the first two IMFs. As reported in the Rao and Lakshmi (Rao and Lakshmi 2015), the instantaneous envelope is expected to show a large spike at the exact time instant of damage. In the present example, the acceleration time history data before and after simulation of the damage (i.e., data realized at 3rd and 4th sec) in the form of minor crack is considered as one data set.
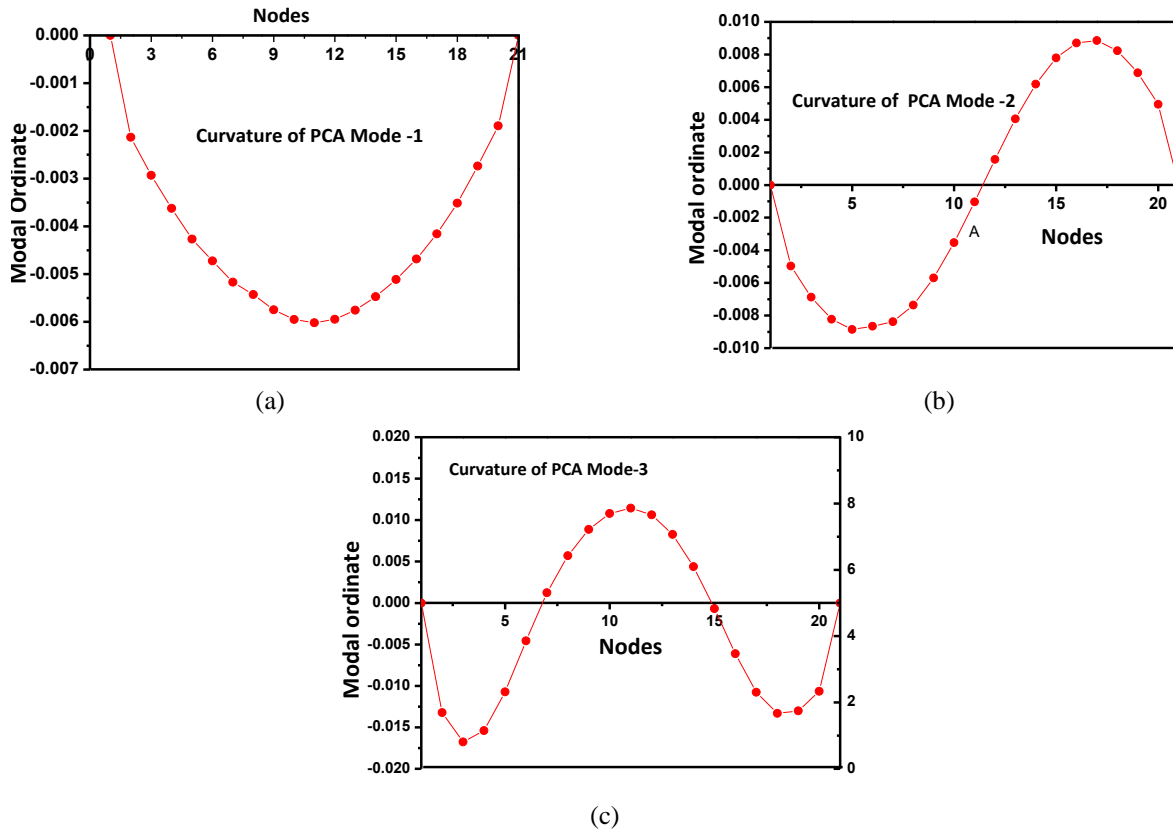
(a)

(b)

(c)

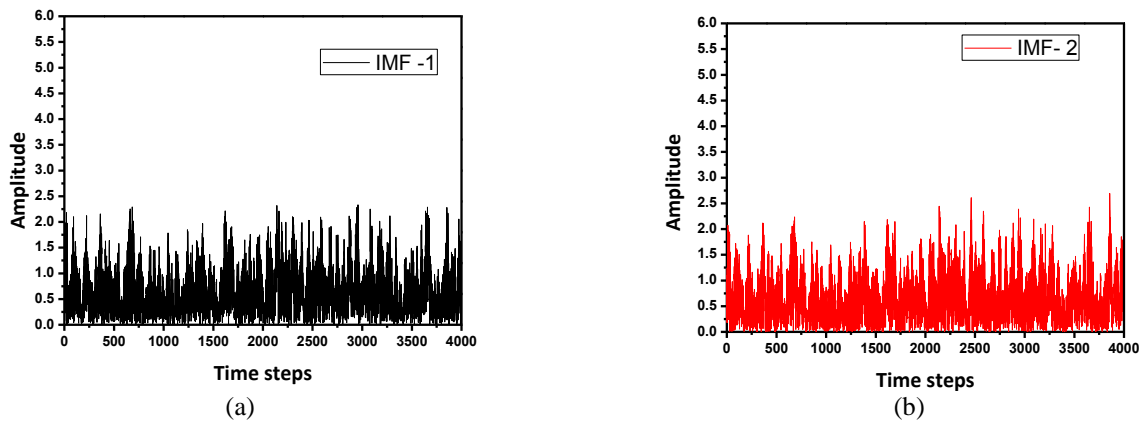Fig. 5 Curvature of the first three PCA modes (test case-1)

(a)

(b)

Fig. 6 Damage detection of test case-1 using HHT: (a) Instantaneous envelope of IMF-1 and (b) Instantaneous envelope of IMF-2

Empirical mode decomposition (EMD) with intermittency criteria is used in the present investigations to generate the intrinsic mode functions (IMFs) from the time history response. Hilbert transform is applied on each of the IMF and the instantaneous envelopments are plotted. It can be easily verified from the plots shown in Fig. 6 that there are multiple smaller spikes all through the time history and no visible major spike to distinguish the exact time instant of damage is observed as popularly reported in the literature. Wavelet analysis is performed on the same data set considered earlier for HHT. We have employed Daubechies wavelet db4 by varying the scale from 1 to 10. The wavelet coefficients for various scale are shown in Fig. 7. We could not observe any distinguishable spike like feature in any one of the scales presented here as popularly reported in Pnevmatikos (Pnevmatikos 2010). Hence it can be concluded from these investigations that neither the multivariate analysis nor the time scale or time-frequency analysis is not been able to detect subtle cracks in the structure.
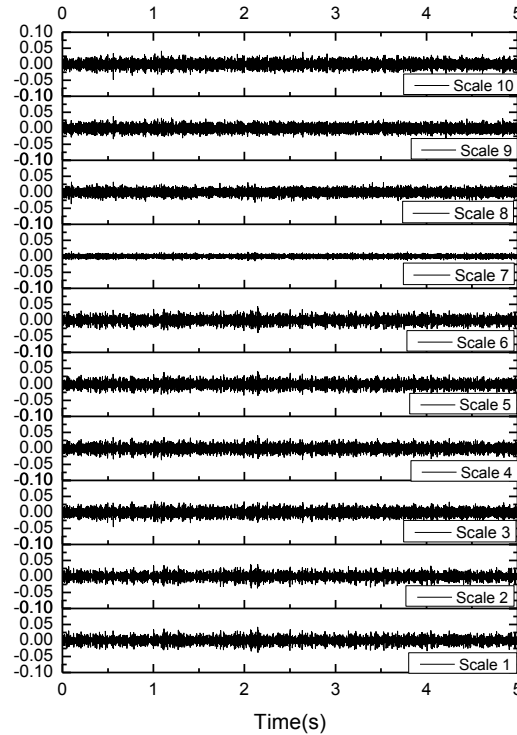
Fig. 7 Wavelet analysis of a subset of test case-1
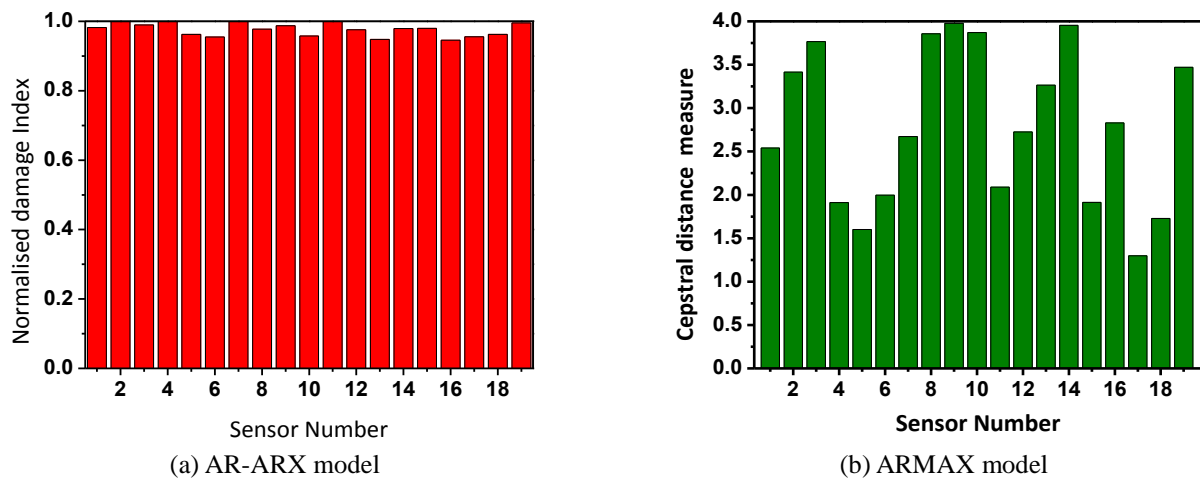

(a) AR-ARX model

(b) ARMAX model

Fig. 8 Damage detection using Time series techniques: (a) AR-ARX models and (b) ARMAX models

A similar exercise has been carried out using time series models also. The damage indices obtained for test case-1 given in Table 1, using AR-ARX model based on the technique outlined in Lakshmi and Rao (Lakshmi and Rao 2015) is shown in Fig. 8(a). Similarly, the damage indices using ARMAX model using Cepstral distance measure (Lakshmi and Rao 2016) as damage index are shown in Fig. 8(b). It is clear from the plots shown in Fig. 8 that time series analysis using either AR-ARX or ARMAX models also fails to detect the minor crack simulated in the structure.

The investigations presented so far on test case-1 clearly indicates that the sensitivity of the popular damage features is not sufficient enough to capture the minor

changes/damage and to reflect them in their indices, even under the normal conditions (i.e., without the environmental variability).

4.1.4 Detection using the proposed technique

In the proposed technique, in order to improve the sensitivity of the time series models, to capture the minor damage, initially, the acceleration time history data (signal) is pre-processed using the EMD with intermittency algorithm, to extract the uni-modal responses, IMFs. It may be noted that the acceleration time-history response is generated afresh with the temperatures, varied from -15 to 50°C, to simulate the effects of environmental variations
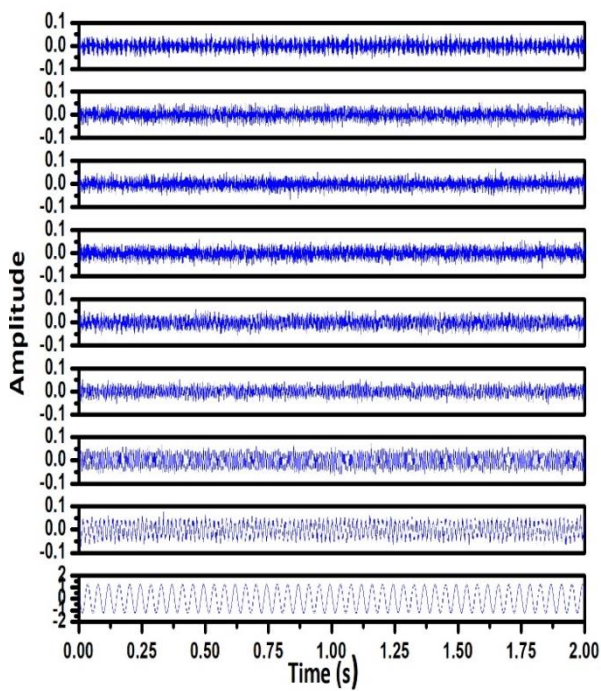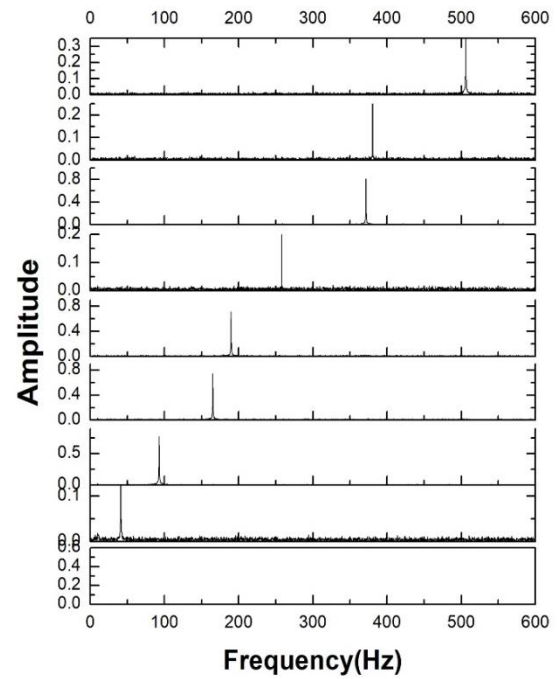
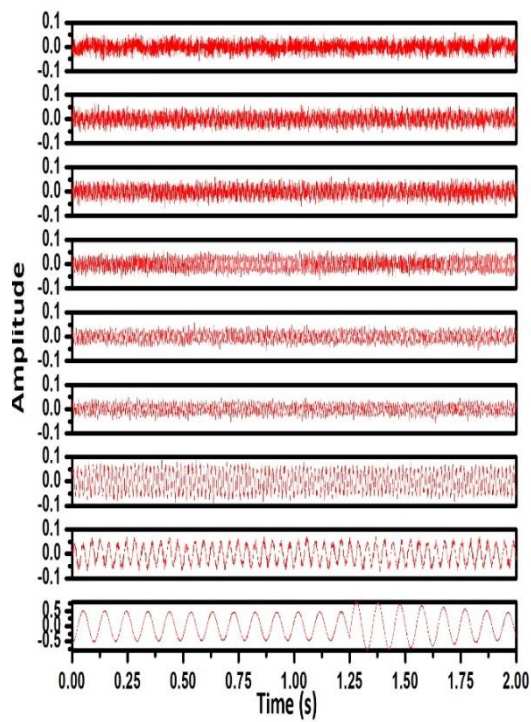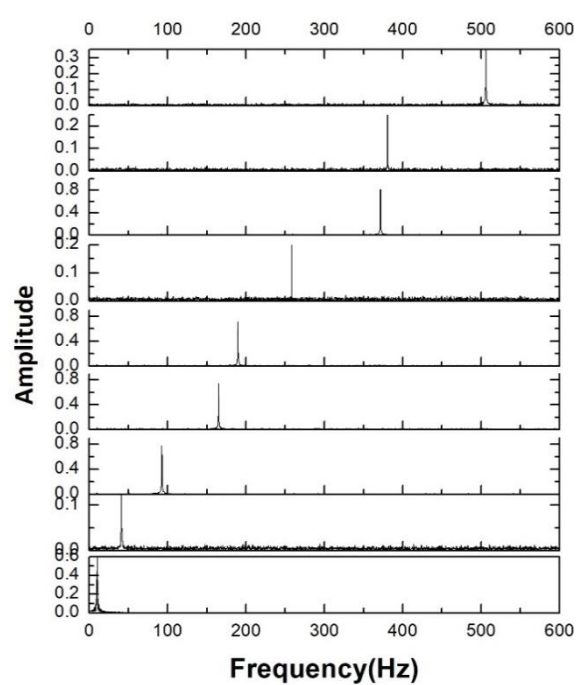(a)   (b)

Fig. 9 EMD of the response at node-6 of simply supported beam-Test Case-1: (a) IMFs of healthy data and (b) FFT spectrum of IMFs of healthy data

(a)   (b)

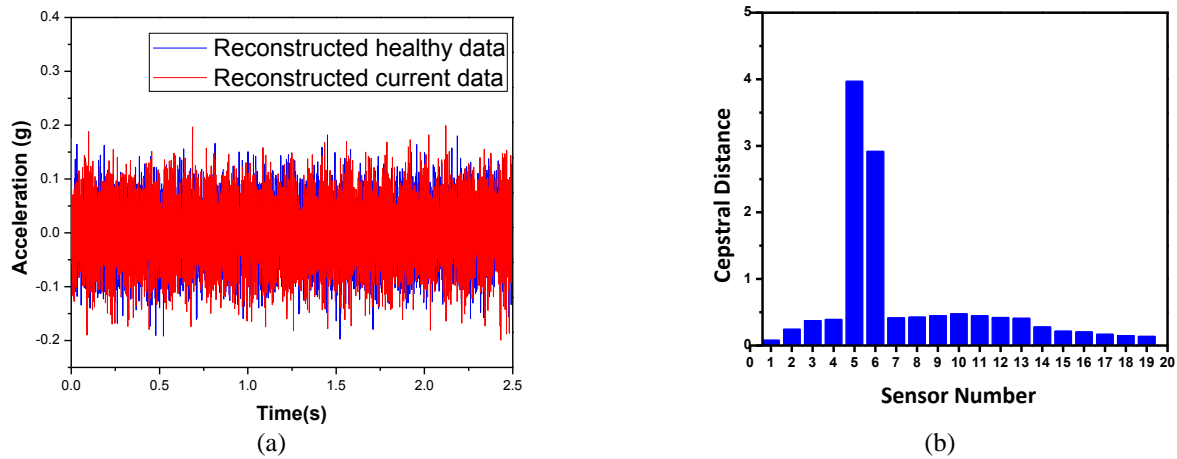Fig. 10 EMD of the response at node-6 of simply supported beam-Test Case-1: (a) IMFs of current data with damage and (b) FFT spectrum of IMFs of current data

Fig. 11 Damage diagnosis of simply supported Beam-Test case-1: (a) Reconstructed signals of healthy and current data of Sensor-6 and (b) Damage index evaluated using cepstral distances of ARMAX models
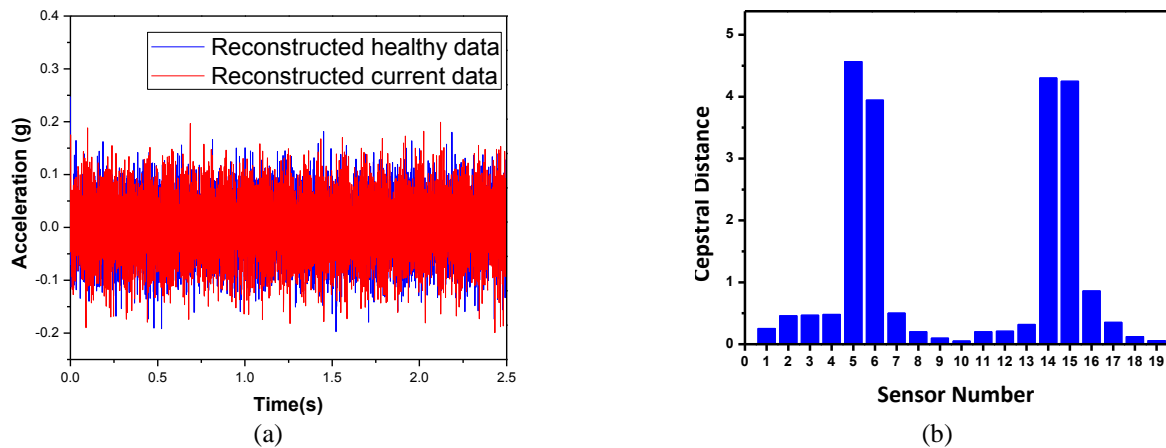

Fig. 12 Damage diagnosis of simply supported Beam-Test case-2: (a) Reconstructed healthy and current data at node-15 and (b) Cepstral distance measure of the reconstructed data

and to test the proposed technique in handling the variability. The details of the IMFs, of both the dynamic signatures obtained from the healthy structure (baseline) and their fast Fourier spectrum(FFT) plots, are shown in Figs. 9(a) and 9(b) respectively. Similarly, the IMFs of the dynamic signatures obtained from the current state of the structure and their FFT plots are shown in Figs. 10(a) and 10(b) respectively.

From the extracted IMFs, damage enriched IMFs are selected using the automated procedure presented in the earlier section. The new current time series is reconstructed using these damage enriched IMFs. In the similar fashion, the new baseline time series is also reconstructed using the already selected IMFs. The typical reconstructed signals of sensor node-6 (i.e., node closer to crack location) using the selected IMFs of the current and healthy signals based on the presence of damage rich features of the current data are shown in Fig. 11(a).

Once the current data subset and the baseline subset are reconstructed using the extracted IMFs, ARMAX model is used to compute the damage indices using cepstral distances

to locate the damage as shown in Fig. 11(b). The results presented in Fig. 11, clearly indicates that the proposed method based on EMD-ARMAX is effective in detecting as well as locating the spatial damage present in the structure in the form of minor crack. Using the count of the current dataset being analyzed, we can arrive at the exact time instant of damage. In this example, the time instant of damage is found to be 3s.

Similarly, the second test case of this numerical example is considered and the results of the investigations are shown in Fig. 12. The spatial location of the two cracks can be easily identified from Fig. 12(b), from the increased damage indices.

From the results, shown in Figs. 9-12, it can be clearly seen that the proposed technique combining EMD and ARMAX model is capable of identifying the location of minor damage like cracks, even in the presence of variability due to environment, operational conditions and measurement noise.
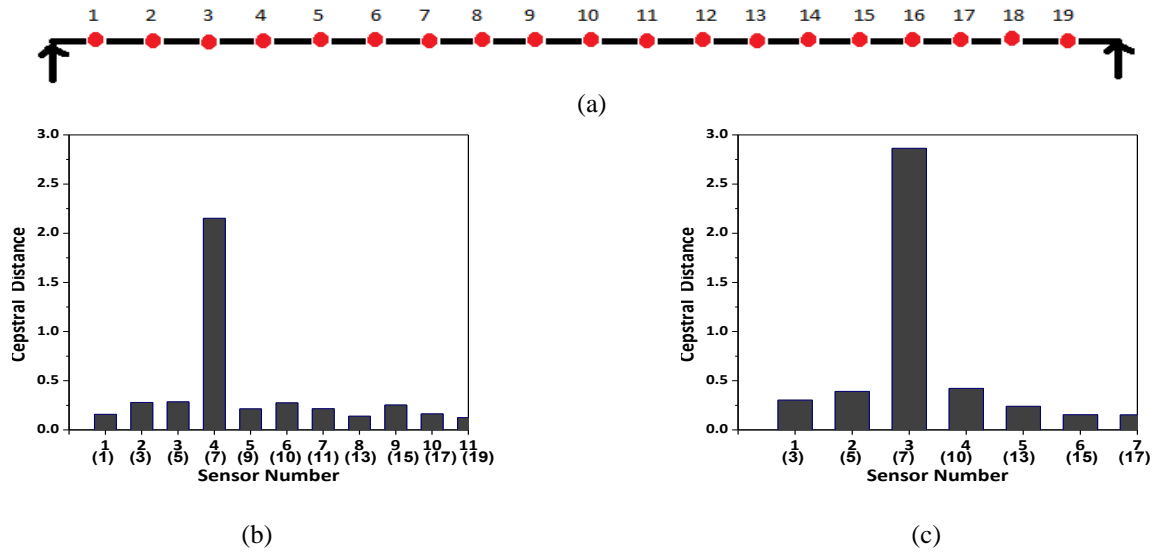
(a)

(b)

(c)

Fig. 13 Damage diagnosis with limited sensor measurements: (a) S.S. beam idealized with complete set of 19 sensors, (b) damage indices of optimally located 11 sensors and (c) damage indices of optimally located 7 sensors

NOTE: The optimal sensor locations are shown in the X-axis of Figs. 13(b)-13(d) and the corresponding original locations with full set of sensors are shown within the brackets

4.1.5 Damage detection using limited measurements

Generally, in practical applications, the sensors available to place on the structure will be limited for the reasons of issues related to cost of the sensory systems and their accessibility. Therefore, it becomes mandatory to place the sensors at optimal limited locations to capture the essential responses from the structure with the minimized cost of SHM system. Mallardo and Alibadi (2013) have proposed various optimal sensor placement techniques. Effective independence (Efi) approach (Kammer 2005, Rama Mohan Rao and Anandakumar 2008) is one of the popular optimal sensor placement techniques and it is adopted in the present study to locate the sensors on the simply supported beam. The final locations of sensors is obtained from Efi and the acceleration time history responses are generated for testcase-1 for those set of sensor nodes with varied temperatures and measurement noise. Considering 11 and 7 numbers of monitoring points, the optimal placement locations on the simply supported beam, identified by Efi, are shown in Table 2.

The damage diagnosis using the proposed technique is carried out with the limited sensor measurements on the optimal locations identified using Efi. The damage indices of the testcase-1 are shown in Figs. 13(b) and 13(c), for 11 and 7 numbers of optimally placed sensors respectively.

Table 2 Optimal locations of sensors on simply supported beam identified using Efi

Number of optimally located sensors	Optimal locations of sensors
11	[1,3,5,7,8,9,10,11,13,15,17,19]
7	[3,5,7,10,13,15,17]

It can be seen clearly from Fig. 13, that the cepstral distances of sensor number 7, placed near the exact damage location (i.e., element no. 6), show the higher magnitude, which indicates the spatial location of damage. Hence, it is proved from this study that the proposed technique can exactly capture the location of the minor cracks with limited number of measurement points located on the structure, handling the effects of temperature variations and the measurement noise.

4.2 Experimental verification:

Laboratory experimental studies are conducted on a simply supported RCC beam to verify the efficiency of the proposed damage detection algorithm using EMD-ARMAX model combined with cepstral distances to locate the minor damage like cracks.

The test structure considered is a simply supported RCC beam with dimensions: span length-300 cm, Width-16.5 cm and Depth-20 cm as shown in Fig. 14. The bottom longitudinal reinforcement was 2# 16 and the upper was 2# 12 with 25# 6 stirrups. The first four natural frequencies of the beam are 28Hz, 112 Hz, 252 Hz and 448 Hz.

Instrumentation of the beam consists of 16 micro-electromechanical systems (MEMS) accelerometers, placed spatially at equal distances along the beam to record the acceleration time history data. The excitation of the beam is performed using a modal shaker of sine peak force capacity of 200N. Tests are carried out using both harmonic as well as random excitations. The loading frequencies, as well as the amplitude, is varied during each set of measurements to simulate operational variability. The time-history of a typical random loading and its frequency spectrum are shown in Figs.16 (a) and 16(b) respectively. To simulate the environmental variability, small masses are arbitrarily
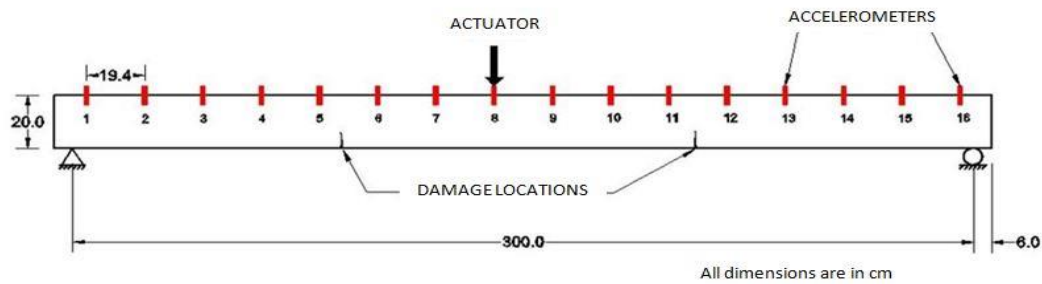
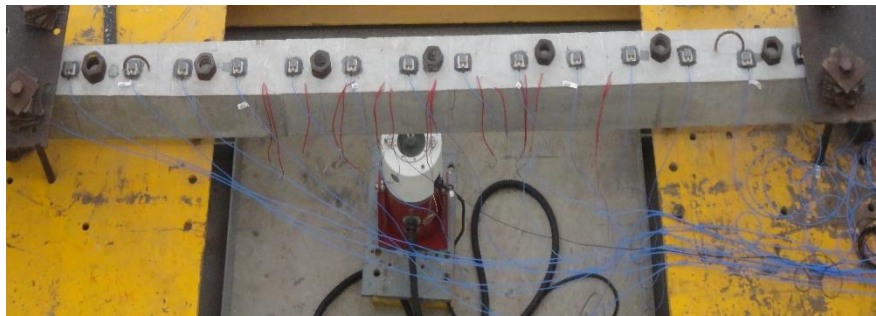Fig. 14 Simply supported RCC beam girder represented schematically

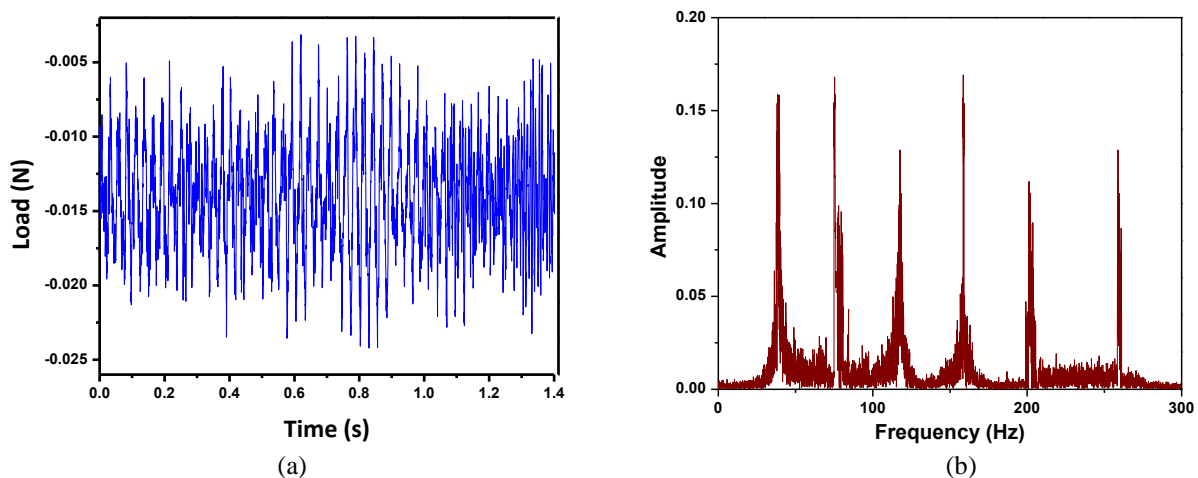Fig. 15 Top view of 'Test setup-1' with added masses for environmental variability

(a)

(b)

Fig. 16 Experimental verification: (a) Typical load time history and (b) Fourier spectrum of load time-history

placed on the beam for each set of measurement. The top view of the beam with added masses is shown in Fig. 15. The experimental setup is named as "Test setup-1". The tests are repeated several times by varying the mass locations in order to simulate environmental variability and also varying the loading on the beam to simulate operational variability.

Initially, acceleration responses of the beam are measured at all the 16 sensor nodes for the undamaged state of the beam. This scenario is named as 'Healthy'. Each signal is measured for 19 sec and is sampled at 3000 Hz.

The damage is inflicted at approximately one-third span from the left side support of the beam (i.e., in element no. 5).

For this purpose, the beam is mounted on a loading frame and in order to inflict cracks at 1/3 span of the beam, the span of the beam is reduced to 2/3rd of the total length of the beam by placing supports on the loading frame accordingly. A hydraulic jack is used to apply static load. The complete experimental arrangement (Test setup-2) with a hydraulic jack, load cell, dial gauge to measure displacements at mid-span (i.e., at the 1/3 span length of the full beam) are shown in Fig. 17.

The static load is applied in small increments. The minor cracks appear at mid-span (i.e., approximately at the 1/3 of the overall span) when the static load applied is 12KN.

Fig. 17 Test setup-2

Fig. 18 Scenario of Damage_Type1

Fig. 19 Scenario of Damage_Type-2

The beam is unmounted from the loading frame at this stage and shifted back to the experimental set-up shown in Fig. 15. At this stage, the beam is having minor cracks developed approximately at 1/3rd span from the left side of the beam and is shown in Fig. 18. The experiment with dynamic excitation force (as discussed earlier for healthy beam) is performed to create test data (acceleration response) of the beam with minor damage and is referred to as 'Damage1'. Similarly, in order to inflict multiple damages on the test specimen, the damage is inflicted using the similar procedure outlined earlier (experimental testsetup_1) at 1/3rd span from right side support (element No: 11) as shown in Fig. 19 and the time history measurements recorded are referred to as 'Damage2'.
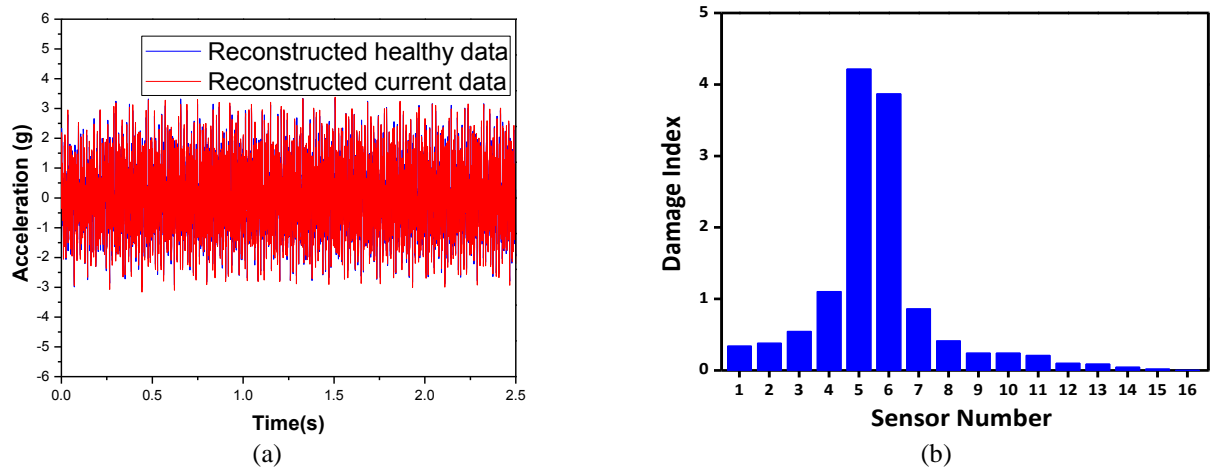
Fig. 20 Damage diagnosis of RCC beam-Single Damage: (a) Reconstructed healthy and current data and (b) Damage index based on Cepstral distances of ARMAX models
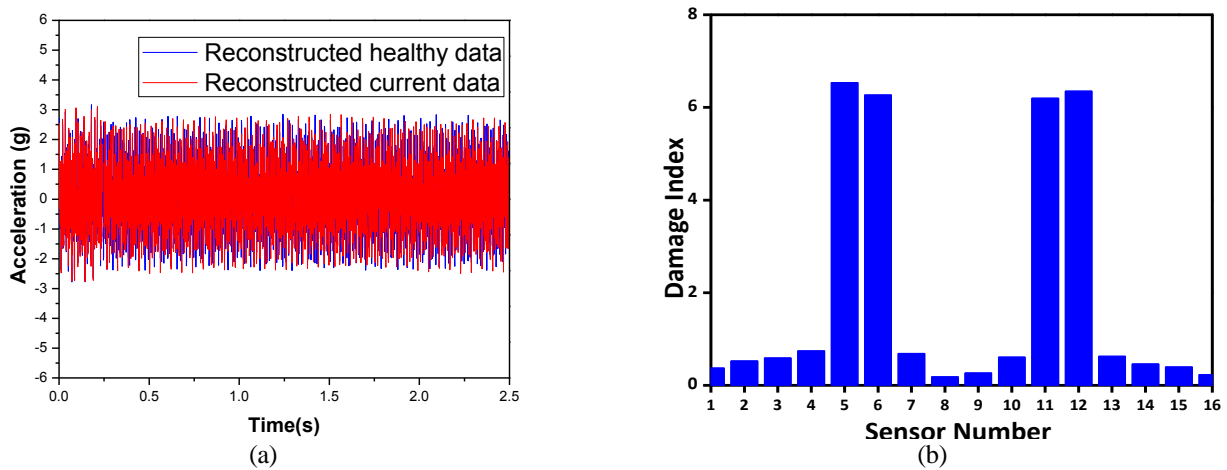

Fig. 21 Damage diagnosis of RCC beam-Multiple Damage: (a) Reconstructed healthy data and current data and (b) Damage index based on cepstral distances of ARMAX models

4.3 Damage diagnosis:

The acceleration data of 'Healthy' is used as the baseline data and the minor damage scenarios – Damage-Type-1 and Damage-Type-2 are used as the current data after the damage has been inflicted. The cross-correlated signals of the measured acceleration time history data of Healthy and Damage-Type-1 are fed to the EMD with intermittency and the IMFs are extracted. The reconstructed signals using the selected IMFs of the current and healthy signals based on the presence of damage rich features of the healthy and current data are shown in Fig. 20(a). The ARMAX models of the reconstructed signals are used to obtain the cepstral distances to locate the damage as shown in Fig. 20(b). The cepstral distance damage indices of ARMAX, for the first damage scenario (single crack at the left 1/3rd span), shown in Fig. 20(b), clearly reflect the spatial location of damage (at one-third of the beam).

Similarly, the IMFs, for the multiple(i.e., two) minor damage scenarios, are obtained and the reconstructed signals are shown in Fig. 21(a). The damage indices obtained from all the sensors are shown in Fig. 21(b). It can be seen clearly from the Fig. 21(b) that the proposed technique can identify the multiple minor damages at the 1/3rd and 2/3rd span of the beam.

The efficiency of the proposed technique is also validated with the limited measurements, obtained from the optimally located measurement points, using Efi. The 8 numbers of optimal sensor locations, identified by Efi, from the original sensor set, are shown in Table 3. The acceleration responses from the optimally located sensor nodes are measured and used for further processing using the proposed technique combining EMD with ARMAX model .
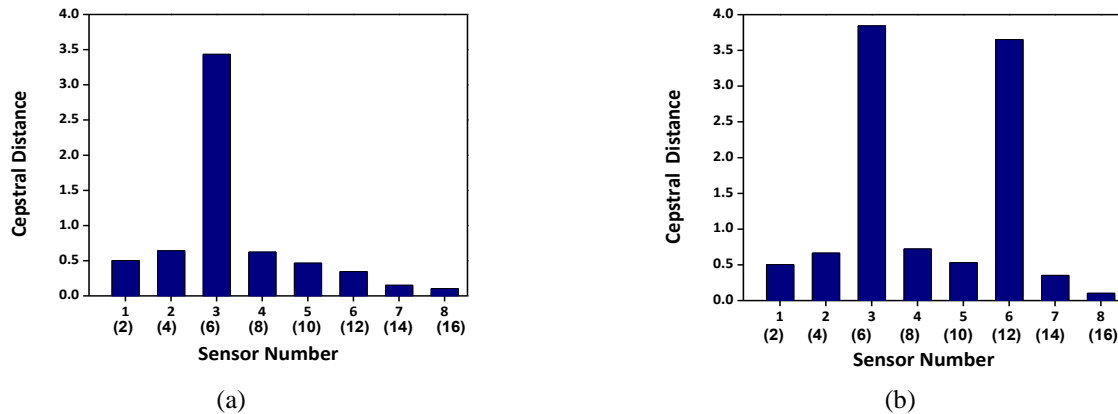
Fig. 22 Results of the experimental studies using RCC beam with limited sensors(8 numbers)   (a) Single Damage scenario and (b) Multiple Damage scenario

NOTE: The optimal sensor locations are shown in the X-axis of Figs. 22(a) and 22(b) and the corresponding original locations with full set of sensors are shown within the brackets

Table 3 Optimal locations of sensors on RCC beam obtained using Efi

Number of optimally located sensors	Optimal locations of sensors
8	[2,4,6,8,10,12,14,16]

The cepstral distance of ARMAX models are evaluated using the optimally placed 8 numbers of sensors and are shown in Fig. 22, for single damage and multiple damage scenarios. The damage indices of sensors 3 and 6 of the optimally arrived sensor set can be observed to have higher magnitudes, indicating the location of the minor cracks, near those sensor locations. It can be noted in Fig. 22, that the optimal sensor locations are shown in the x-axis and the original sensor node number is shown within the brackets. From the results of Fig. 22, it can be clearly seen that the proposed damage diagnosis technique, can identify the precise spatial location of the minor damages, using limited number of sensors and also handling the influences of variability due to environment/operational conditions and measurement noise.

5. Conclusions

It is shown in this paper that the minor changes in the dynamic characteristics of the structures, due to the minor cracks developed in the structure, alter only some specific modal responses while rest of the modal responses contributing to the overall response will not get altered. Hence, the damage features present in the modal responses of specific modes which are affected by the minor incipient damage will be hidden in the overall response (i.e., the measured dynamic signature), which is basically the summation of all contributory modal responses. Apart from this, noise also masks the minor incipient damages present in the structure. Keeping this in view, an attempt has been made to isolate these damage sensitive modal responses and

reconstruct the signal accordingly using an automated algorithm, based on EMD.

Empirical mode decomposition is performed on the cross-correlated acceleration time history response. In order to obtain IMFs without mode mixing and also handle the systems with closely spaced modes in the signal, EMD procedure with intermittency criteria is also proposed in this paper.   The damage enriched signals isolated by EMD are further used for damage diagnosis using the ARMAX model. Numerical simulation studies have been carried out by considering a simply supported beam with minor cracks. Laboratory experimental studies have been carried out by considering an RCC beam to complement the numerical simulations and also demonstrate its practical applicability. The following conclusions are drawn based on the investigations carried out and presented in this paper.

i.   EMD with intermittency criteria, performed on the cross-correlated signals is found to be effective for the problems considered in this paper.

ii.   An approach to automatically identify and isolate the modal responses with damage rich features is found to be effective.

iii.   Numerical and experimental studies carried out and presented in this paper clearly indicate that the proposed damage diagnostic method is highly immune to noise and can robustly identify smaller cracks developed in the structure at their incipient stage.

iv.   In civil engineering structures, the environmental and operational variabilities often mislead the damage diagnostic process, especially when the damages present in the structure are subtle. Hence, the changes in the dynamic features due to the effect of variability and the minor structural damage need to be distinguished. In this paper, it is shown through numerical and experimental investigations, that, while, the ARMAX model with matching procedure can effectively isolate the effects of environmental and operational variability, the hybrid damage diagnostic procedure combining EMD with ARMAX model can identify the change in the dynamic features due to minor/subtle cracks in the structure.

v. The proposed hybrid damage diagnostic algorithm combining EMD with ARMAX is highly amenable for online monitoring of structures.

Acknowledgments

References

Arhant, M., Meek, N., Penumadu, D. *et al.* (2018), "Residual strains using integrated continuous fiber optic sensing in thermoplastic composites and structural health monitoring", *Exp. Mech.*, **58**(1), 167-176.

Avendaño-Valencia, L.D. and Fassois, S.D. (2015), "Natural vibration response based damage detection for an operating wind turbine via Random Coefficient Linear Parameter Varying AR modelling", *J. Physics: Conference Series*, **628**(1), 012073, IOP Publishing.

Bodeux, J.B. and Golinval, J.C. (2001), "Application of ARMAV models to the identification and damage detection of mechanical and civil engineering structures", *Smart Mater. Sstruct.*, **10**(3), 479-489.

Coughlin, K. and Tung, K.K. (2005), "Empirical mode decomposition and climate variability", *In Hilbert–Huang Transform and its Applications*, 223-239, Interdisciplinary Mathematical Sciences.

Das, S., Saha, P. and Patro, S.K. (2016), "Vibration-based damage detection techniques used for health monitoring of structures: a review", *J. Civil Struct. Health Monit.*, **6**(3), 477-507.

Doebling, S.W., Farrar, C.R. and Prime, M.B. (1998), "A summary review of vibration-based damage identification methods", *Shock Vib. Dig.*, **30**(2), 91-105.

Dorvash, S., Pakzad, S.N. and LaCrosse, E.L. (2014), "Statistics based localized damage detection using vibration response", *Smart Struct. Syst.*, **14**(2), 85-104.

Dosiek, L. and Pierre, J.W. (2013), "Estimating electromechanical modes and mode shapes using the multichannel ARMAX model", *IEEE T. Power Syst.*, **28**(2), 1950-1959.

Fan, X., Li, J. and Hao, H. (2016), "Piezoelectric impedance based damage detection in truss bridges based on time frequency ARMA model", *Smart Struct. Syst.*, **18**(3), 501-523.

Farrar, C.R., Sohn, H. and Worden, K. (2001), "Data normalization: a key for structural health monitoring",No. LA-UR-01-4212, Los Alamos National Laboratory.

Fassois, S.D. and Sakellariou, J.S. (2007), "Time-series methods for fault detection and identification in vibrating structures", *Philosophical Transactions of the Royal Society of London A: Mathematical, Physical and Engineering Sciences*, **365**(1851), 411-448.

Fassois, S.D. and Sakellariou, J.S. (2009), "Statistical time series methods for SHM", *Encyclopedia of structural health monitoring*.

Foti, S. and Sabia, D. (2010), "Influence of foundation scour on the dynamic response of an existing bridge", *J. Bridge Eng.*, **16**(2), 295-304.

Fugate, M.L., Sohn, H. and Farrar, C.R. (2001), "Vibration-based damage detection using statistical process control", *Mech. Syst. Signal Pr.*, **5**(4), 707-721.

Gao, Y., Ge, G., Sheng, Z. *et al.* (2008), "Analysis and solution to the mode mixing phenomenon in EMD", *Image and Signal Processing*, (CISP'08), **5**, 223-227, IEEE.

Golinval, J.C. (2017), "Damage detection in structures based on principal component analysis of forced harmonic responses", *Procedia Eng.*, **199**, 1912-1918.

Hsu, W.K., Chiou, D.J., Chen, C.W., Liu, M.Y., Chiang, W.L. and Huang, P.C. (2014), "A case study of damage detection in four-bays steel structures using the HHT approach", *Smart Struct. Syst.*, **14**(4), 595-615.

Hu, M.H., Tu, S.T. and Xuan, F.Z. (2015), "Statistical moments of ARMA (n, m) model residuals for damage detection", *Procedia Eng.*, **130**, 1622-1641.

Huang, N.E. (2005), "Introduction to Hilbert-Huang transform and some recent developments", *Hilbert-Huang Transform in Engineering*. Taylor & Francis, Boca Raton, 1-24.

Huang, N.E. (2014), "Hilbert-Huang transform and its applications", **16**, World Scientific Publishing Company.

Jayawardhana, M., Zhu, X., Liyanapathirana, R. *et al.* (2015), "Statistical damage sensitive feature for structural damage detection using AR model coefficients", *Adv. Struct. Eng.*, **18**(10), 1551-1562.

Kammer , D.C. (2005), "Sensor set expansion for modal vibration testing", *Mech. Syst. Signal Pr.*, **19**(4), 700-713.

Kopsaftopoulos, F.P. and Fassois, S.D. (2015), "A vibration model residual-based sequential probability ratio test framework for structural health monitoring", *Struct. Health Monit.*, **14**(4), 359-381.

Kostić, B. and Gül, M. (2017), "Vibration-based damage detection of bridges under varying temperature effects using time-series analysis and artificial neural networks", *J. Bridge Eng.*, **22**(10), 04017065.

Kraemer, P. (2011), "Damage diagnosis approaches for structural health and condition monitoring of offshore wind energy plants", University of Siegen, Siegen, Germany.

Krawczuk, M., Żak, A. and Ostachowicz, W. (2000), "Elastic beam finite element with a transverse elasto-plastic crack", *Finite Elem. Anal. Des.*, **34**(1), 61-73.

Lakshmi, K. and Rama Mohan Rao, A. (2014), "A robust damage-detection technique with environmental variability combining time-series models with principal components", *Nondestruct.Test. Eval.*, **29**(4), 357-376.

Lakshmi, K. and Rao, A. (2015), "Damage identification technique based on time series models for LANL and ASCE benchmark structures", *Insight-Non-Destruct. Test. Condition Monit.*, **57**(10), 580-588.

Lakshmi, K. and Rao, A.R.M. (2016), "Structural damage detection using ARMAX time series models and cepstral distances", *Sādhanā*, **41**(9), 1081-1097.

Lu, Y. and Gao, F. (2005), "A novel time-domain auto-regressive model for structural damage diagnosis", *J. Sound Vib.*, **283**(3-5), 1031-1049.

Mallardo, V. and Alibadi M.H. (2013), "Optimal sensor placement for structural damage and impact identification- A review", *Struct. Durability Health Monit.*, **9**(4), 287-323.

Mosavi, A.A., Dickey, D., Seracino, R. *et al.* (2012), "Identifying damage locations under ambient vibrations utilizing vector autoregressive models and Mahalanobis distances", *Mech. Syst. Signal Pr.*, **26**, 254-267.

Nair, K.K., Kiremidjian, A.S. and Law, K.H. (2006), "Time series-based damage detection and localization algorithm with application to the ASCE benchmark structure", *J. Sound Vib.*, **291**(1-2), 349-368.

Oppenheim, A.V. and R. W. Schafer (1975), "Digital Signal Processing", Prentice-Hall, Englewood Cliffs, New Jersey, **6**, 125-136.

Pandit, S.M. and Wu, S.M. (1983), "Time series and system analysis with applications", (Vol. **3**). New York: Wiley.

Pnevmatikos, N. (2010), "Damage detection of structures using discrete wavelet transform", *Proceedings of the 5th World*

Conference on Structural Control and Monitoring.

Pnevmatikos, N.G., Blachowski, B., Hatzigeorgiou, G.D. and Swiercz, A. (2016), "Wavelet analysis based damage localization in steel frames with bolted connections", *Smart Struct. Syst.*, **18**(6), 1189-1202.

Rao A.R.M. and Anandakumar, G. (2008), "Optimal sensor placement techniques for system identification and health monitoring of civil structures", *Smart Struct. Syst.*, **4**(4), 465-492.

Rao, A.R.M. and Lakshmi, K. (2015), "Damage diagnostic technique combining POD with time-frequency analysis and dynamic quantum PSO", *Meccanica*, **50**(6), 1551-1578.

Rao, A.R.M., Lakshmi, K. and Krishna Kumar, S. (2015), "Detection of delamination in laminated composites with limited measurements combining PCA and dynamic QPSO", *Adv. Eng. Softw.*, **86**, 85-106.

Rosales, M.J. and Liyanapathirana, R. (2017), "Data driven innovations in structural health monitoring", *J. Phys.: Conference Series*, **842**(1), 012012, IOP Publishing.

Sakaris, C.S., Sakellariou, J.S. and Fassois, S.D. (2015), "A Generalized Functional Model Based Method for Vibration-Based Damage Precise Localization in 3D Structures", *J. Physics: Conference Series*, **628**(1), 012008, IOP Publishing.

Sakaris, C.S., Sakellariou, J.S. and Fassois, S.D. (2017), "Random-vibration-based damage detection and precise localization on a lab–scale aircraft stabilizer structure via the generalized functional model based method", *Struct. Health Monit.*, **16**(5), 594-610.

Shen, S.S.P., Shu, T., Huang, N.E. *et al.* (2005), "HHT analysis of the nonlinear and non-stationary annual cycle of daily surface air temperature data", *In Hilbert–Huang Transform and Its Applications*, 187-209, Interdisciplinary Mathematical Sciences.

Sohn, H. and Farrar, C.R. (2001), "Damage diagnosis using time series analysis of vibration signals", *Smart Mater. Struct.*, **10**(3), 446-451.

Tanner, N.A., Wait, J.R., Farrar, C.R. *et al.* (2003), "Structural health monitoring using modular wireless sensors", *J. Intel. Mat. Syst. Str.*, **14**(1), 43-56.

Ugalde, U., Anduaga, J., Martínez, F. *et al.* (2015), "Novel SHM method to locate damages in substructures based on VARX models", *J. Phys.: Conference Series*, **628**(1), 012013, IOP Publishing.

Xie, L. and Mita, A. (2017), "An innovative substructure damage identification approach for shear structures based on ARMAX models", *Procedia Eng.*, **188**, 119-124.

Zhang, Q.W. (2007), "Statistical damage identification for bridges using ambient vibration data", *Comput. Struct.*, **85**(7-8), 476-485.

BS

Appendix-A

ARMAX model

The ARMAX model is preferred in this proposed technique because it includes the dynamics of the disturbance also unlike the other time series models. An ARMAX process of a healthy data, $x(t)$ is given below.

$$
x(t) = \sum_{i=1}^{p} \alpha_i x(t-i)
$$

$$
+ \sum_{i=1}^{q} \beta_i u(t-n_k-i) \qquad \text{(A.1)}
$$

$$
+ \sum_{i=1}^{b} \delta_i \varepsilon(t-i) + \varepsilon(t)
$$

where ε is the error between the measured signal and the output from the prediction model and n_k is the time delay, which, in this case, is set to 1. α_i, β_i and δ_i, are the parameters of AR, exogenous input(u) and MA models respectively. p, q and b are the orders of AR exogenous and MA parts respectively. The input series, u, is the acceleration time history signals of adjacent sensor nodes while fitting an ARMAX model to the data from a sensor node.

Cepstral distance based damage index

The damage index is based on the cepstral distances between the ARMAX models of the healthy and current data subsets reconstructed using the selected few IMFs. The cepstral distance is the weighted Euclidean distance between the power cepstrum of ARMAX models of the two subsets.

The power cepstrum is nothing but the logarithm of the power spectrum $P(z)$, subjected to inverse Fourier transform (Oppenheim and Schafer 1975)

$$
\log P(z) = \log\{\sigma^2 \, \mathrm{H}(z)\overline{\mathrm{H}}(z^{-1})\}
$$

$$
= \sum_{k \in Z} cc(k) z^{-k} \qquad \text{(A.2)}
$$

Where $cc(k)$ are the cepstrum coefficients, σ^2 is the variance of the white noise process possessing zero-mean and $H(z)$ is the transfer function of the system.

An ARMAX process at time 'k' is represented as follows

$$
A(q^{-1})x[k] = B(q^{-1})u[k-n_k]
$$

$$
+ C(q^{-1})e_x[k] \qquad \text{(A.3)}
$$

In Z domain, the transfer function of the system's ARMAX process can be represented in the following form (Dosiek and Pierre 2013)

$$
H(Z) = [A^{-1}(Z)B(Z) \quad A^{-1}(Z)C(Z)] \qquad \text{(A.4)}
$$

$$
\textit{where } A^{-1}(q) = \frac{1}{|A(q)|} adj[A(q)];
$$

$A(q) = I + A_1 q^{-1} + \ldots + A_{na} q^{-na}$ is the AR polynomial matrix; $B(q) = B_0 + B_1 q^{-1} + \ldots + B_{nb} q^{-nb}$ is the input polynomial matrix and $C(q) = I + C_1 q^{-1} + \ldots + C_{nc} q^{-nc}$ is the MA polynomial matrix with orders na, nb and nc respectively.

A close look at the second part of the transfer function shows the AR and MA components of the system. If these components are in terms of poles $\alpha(i)$ and zeros $\beta(i)$, the transfer function resembles that of a stable, minimum ARMA process in the Z-domain as

$$
H(z) = \frac{\sum_{i=0}^{nc} c(i) z^{-i}}{\sum_{i=0}^{na} \mathrm{a}(i) z^{-i}} = \frac{\prod_{i=1}^{nc}(1-\beta(i)z^{-i})}{\prod_{i=1}^{na}(1-\alpha(i)z^{-i})} \qquad \text{(A.5)}
$$

Therefore, now, for any two ARMAX models AM_1, and AM_2, with the corresponding cepstrum coefficients $cc_1(n)$ and $cc_2(n)$, the cepstral distance becomes the Euclidean distance between the cepstrums

$$
d(AM_1, AM_2)^2 = \sum_{n=1}^{\infty} n |cc_1(n) - cc_2(n)|^2 \qquad \text{(A.6)}
$$

where $cc(n)$ are the coefficients of the cepstrum given in terms of poles and zeros

$$
cc(n) = \begin{cases} \frac{1}{|n|}\left\{\sum_{i=1}^{p} \alpha^{|n|}(i) - \sum_{i=1}^{q} \beta^{|n|}(i)\right\}, n \neq 0 \\ \log \sigma^2, \, n = 0 \end{cases} \qquad \text{(A.7)}
$$

This measure of distance evaluated from Eq. (A.6) is used for damage localization and is calculated for all the sensor nodes independently. Once the damage index (cepstral distance) of the subset for all the sensor nodes are obtained, it is investigated for the location of damage. The cepstral distance increases with the increase in the difference between any two signals considered for investigation. Therefore, the value of higher damage index at a sensor node is considered to be an indication of the existence of damage near that node on the structure. Also, the time instant of damage can be calculated from the subset index number. Therefore, this damage detection methodology combining EMD and ARMAX model using the cepstral damage index can act as a good localization metric, which gives a picture of change of state of the structure under each sensor signal without the correlations of excitations spatially.

Appendix-B

Formulations of stiffness and mass matrix for a cracked beam

A beam of cross-section B and D, with a crack of length 'L' in a selected element of length 'l' , is shown in Figure B.1. For the cracked element, there are three different parts, namely, left uncracked segment, crack segment and right uncracked segment.
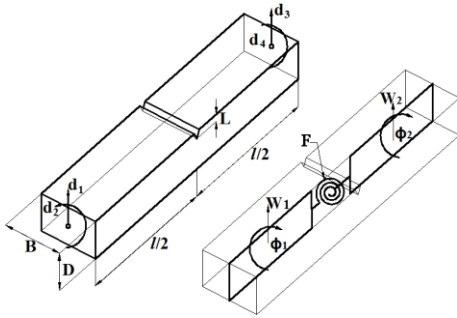

Fig. 1 Finite element of a cracked beam

The left and right segments are modelled as non-cracked beams with length L/2 and the crack segment is modelled as a spring with zero mass and length. Every beam element hasa transverse displacement and a rotation in each node. Elasto-plastic fracture mechanics (EFEM) is used to model the crack where the effect of plasticity at the crack tip is also considered (Krawczuk *et al.* 2000).The effect of the local flexibility which arises due to the existence of crack is also modelled in the stiffness of the torsional spring. At the cracked cross-section of the beam, the flexibility can be written as

$$F = \frac{72}{EBD^2} \int_0^{\bar{L}_k} c(\bar{L})^2 \bar{L} d\bar{L}$$

$$+ \frac{216}{E\pi BD^2} \left(\frac{f}{f_y}\right)^2 \int_0^{\bar{L}_k} c(\bar{L})^4 \bar{L} d\bar{L},$$ (B.1)

Where;

$$C = \sqrt{\frac{tan(\pi L/2D)}{\pi L/2D} \frac{0.923 + 0.199[1 - sin(\pi L/2D)]^4}{cos(\pi L/2D)}};$$

f is the applied nominal stress, f_y is the yield strength of the material and E is Young's modulus.

The mass matrix of the cracked element is given as

$$M_c = \frac{\rho Al}{420} M_e^t + \rho IlM_e^r,$$ (B.2)

where M_e^t represents the portion of inertia matrix related to the transverse motion and M_e^r is the portion of inertia matrix related to the rotation motion given as

$$M_e^t = \begin{bmatrix} 156 & \frac{l^2(88l+123\bar{K})}{4(l+\bar{K})} & 54 & -\frac{l^2(52l+87\bar{K})}{4(l+\bar{K})} \\ & \frac{l^3(64l^2+191l\bar{K}+148\bar{K}^2)}{16(l+\bar{K})^2} & \frac{l^2(52l+87\bar{K})}{4(l+\bar{K})} & \frac{3l^3(16l^2+53l\bar{K}+44\bar{K}^2)}{16(l+\bar{K})^2} \\ & & 156 & -\frac{l^2(88l+123\bar{K})}{4(l+\bar{K})} \\ sym & & & \frac{l^3(64l^2+191l\bar{K}+148\bar{K}^2)}{16(l+\bar{K})^2} \end{bmatrix},$$

$$M_e^r = \begin{bmatrix} \frac{6}{5l^2} & \frac{1}{10l} & -\frac{6}{5l^2} & \frac{1}{10l} \\ & \frac{l(8l^2+21l\bar{K}+18\bar{K}^2)}{60(l+\bar{K})^2} & -\frac{1}{10l} & -\frac{l(8l^2+21l\bar{K}+18\bar{K}^2)}{60(l+\bar{K})^2} \\ & & \frac{6}{5l^2} & -\frac{1}{10l} \\ sym & & & \frac{l(8l^2+21l\bar{K}+18\bar{K}^2)}{60(l+\bar{K})^2} \end{bmatrix},$$

Where $\bar{K} = EIF$; I represents the geometrical moment of inertia of the cross-section of the beam and A is the area of the cross-section of the beam. It can be seen that at the crack location, the elements of the inertia matrix is a function of the flexibility coefficient $\bar{K}$ and when the inertia matrix is similar to the non-cracked element.

The element stiffness matrix is given by

$$K_e = EI \begin{bmatrix} \frac{12}{l^3} & \frac{6}{l^2} & -\frac{12}{l^3} & \frac{6}{l^2} \\ & \frac{4l^2+6l\bar{K}+3\bar{K}^2)}{l(l+\bar{K})^2} & -\frac{6}{l^2} & \frac{2l^2+6l\bar{K}+3\bar{K}^2)}{l(l+\bar{K})^2} \\ & & \frac{12}{l^3} & -\frac{6}{l^2} \\ sym & & & \frac{4l^2+6l\bar{K}+3\bar{K}^2)}{l(l+\bar{K})^2} \end{bmatrix},$$ (B.3)

It can be seen from the above equation of the stiffness matrix of the element that, when $\bar{K} = 0$, the stiffness matrix becomes the same as that of the non-cracked element.